Mon. Not. R. Astron. Soc. **000**, 000–000 (0000) Printed 7 August 2012 (MN LATEX style file v2.2)

Galaxy clustering as dark energy probe: baryon acoustic oscillations and beyond

Yun Wang⋆

Homer L. Dodge Department of Physics & Astronomy, Univ. of Oklahoma, 440 W Brooks St., Norman, OK 73019, U.S.A.

7 August 2012

ABSTRACT

Galaxy clustering is one of the most powerful probes of the true nature of the observed cosmic acceleration. It contains baryon acoustic oscillations (BAO) that are cosmological standard rulers calibrated by the cosmic microwave background anisotropy data. The BAO allows us to measure the cosmic expansion history directly. Beyond the BAO, the full shape of galaxy clustering (either in the measured galaxy power spectrum or the galaxy correlation function) provides significantly more cosmological information, and in particular, allows us to test deviations from general relativity via the redshift space distortions. Here we introduce the basic ideas and analysis techniques for using galaxy clustering data to constrain dark energy and test gravity. We examine the critical issues, current status, as well as future prospects.

Since the 1980s, galaxy redshift surveys have been used to map the large scale structure in the universe, and constrain cosmological parameters. Galaxy redshift surveys are powerful as dark energy probe, since they can allow us to measure the cosmic expansion history $H(z)$ through the measurement of baryon acoustic oscillations (BAO) in the galaxy distribution, and the growth history of cosmic large scale structure $f_g(z)$ through independent measurements of redshift-space distortions and the bias factor between the distribution of galaxies and that of matter (Wang 2008).

1 BARYON ACOUSTIC OSCILLATIONS AS STANDARD RULER

The use of BAO as a cosmological standard ruler is a relatively new method for probing dark energy (Blake & Glazebrook 2003; Seo & Eisenstein 2003), but it has already yielded impressive observational results (Eisenstein et al. 2005).

Measuring $H(z)$ and $D_A(z)$ from BAO

At the last scattering of CMB photons, the acoustic oscillations in the photon-baryon fluid became frozen, and imprinted their signatures on both the CMB (the acoustic peaks in the CMB angular power spectrum) and the matter distribution (the baryon acoustic oscillations in the galaxy power spectrum). Because baryons comprise only a small fraction of matter, and the matter power spectrum has evolved significantly since last scattering of photons, BAO are much smaller in amplitude than the CMB acoustic peaks, and are washed out on small scales.

BAO in the observed galaxy power spectrum have the characteristic scale determined by the comoving sound horizon at the drag epoch (shortly after photon-decoupling), which is precisely measured by the CMB anisotropy data (Page 2003; Spergel et al. 2007; Komatsu et al. 2009). The observed BAO scales appear as slightly preferred redshift separation $s_\parallel$ and angular separation $s_\perp$:

$$s_\parallel \propto sH(z), \qquad s_\perp \propto \frac{s}{D_A(z)}, \tag{1}$$

where s is the sound horizon scale at the drag epoch, and the angular diameter distance $D_A(z) = r(z)/(1+z)$, with $r(z)$ denoting the comoving distance given by

$$r(z) = cH_0^{-1}\,|\Omega_k|^{-1/2}\mathrm{sinn}[|\Omega_k|^{1/2}\,\Gamma(z)], \tag{2}$$
$$\Gamma(z) = \int_0^z \frac{dz'}{E(z')}, \qquad E(z) = H(z)/H_0$$

where $\mathrm{sinn}(x) = \sin(x)$, x, $\sinh(x)$ for $\Omega_k < 0$, $\Omega_k = 0$, and $\Omega_k > 0$ respectively. Thus comparing the observed BAO scales with the expected values gives $H(z)$ in the radial direction, and $D_A(z)$ in the transverse direction.

Calibration of the BAO Scale

CMB data give us the comoving sound horizon at photon-decoupling epoch (Eisenstein & Hu 1998; Page 2003)

$$\begin{aligned} r_s(z_*) &= \int_0^{t_*} \frac{c_s\,dt}{a} = H_0^{-1}\int_{z_*}^{\infty} dz\,\frac{c_s}{E(z)} \\ &= cH_0^{-1}\int_0^{a_*} \frac{da}{\sqrt{3(1+R_b)\,a^4E^2(z)}}, \end{aligned} \tag{3}$$

where a is the cosmic scale factor, $a_* = 1/(1+z_*)$, and

$$a^4E^2(z) = \Omega_m(a+a_{\rm eq}) + \Omega_k a^2 + \Omega_X X(z) a^4, \tag{4}$$

where the dark energy density function $X(z) \equiv \rho_X(z)/\rho_X(0)$, and the cosmic scale factor at the epoch of matter and radiation equality is given by

$$a_{\rm eq} = \frac{\Omega_{\rm rad}}{\Omega_m} = \frac{1}{1+z_{\rm eq}}, \qquad z_{\rm eq} = 2.5{\times}10^4\Omega_m h^2\left(\frac{T_{CMB}}{2.7\,\mathrm{K}}\right)^{-4}. \tag{5}$$

We have assumed three massless neutrino species, so that the radi-

© 0000 RAS

ation energy density today is (Kolb & Turner 1990)

$$\rho_{rad}^0 = \frac{\pi^2}{30}\, g_*^0 T_{CMB}^4,$$
$$g_*^0 = 2 + \frac{7}{8} \times 2 \times 3 \times \left(\frac{4}{11}\right)^{4/3} \quad (6)$$

The sound speed c_s and the baryon/photon ratio R_b are given by

$$c_s^2 \equiv \frac{\delta p}{\delta \rho} \simeq \frac{c^2 \delta\rho_\gamma/3}{\delta\rho_\gamma + \delta\rho_b} = \frac{c^2}{3\,(1+\dot\rho_b/\dot\rho_\gamma)} = \frac{c^2}{3(1+R_b)} \quad (7)$$
$$R_b \equiv \frac{3\rho_b}{4\rho_\gamma} \equiv \overline{R_b}\, a, \qquad \overline{R_b} = 31500\Omega_b h^2 \left(\frac{T_{CMB}}{2.7\,\mathrm{K}}\right)^{-4}. \quad (8)$$

We have used $\rho_\gamma \propto a^{-4}$ and $\rho_b \propto a^{-3}$.

COBE four year data give $T_{CMB} = 2.728 \pm 0.004\,\mathrm{K}$ (95% C.L.) (Fixsen et al. 1996). The data from WMAP 5 year observations give the redshift and the sound horizon at the photon-decoupling epoch

$$z_* = 1090.51 \pm 0.95, \qquad r_s(z_*) = 146.8 \pm 1.8\,\mathrm{Mpc}, \quad (9)$$

assuming $T_{CMB} = 2.725$ (Komatsu et al. 2009). The BAO scale measured in galaxy redshift surveys correspond to the sound horizon scale at the *drag epoch* (Hu & Sugiyama 1996).

The drag epoch occurs when the photon pressure (or "Compton drag") can no longer prevent gravitational instability in the baryons. Thus there is no reason for the photon-decoupling epoch, z_*, to be the same as the drag epoch, z_d. The scattering in the photon/baryon fluid leads to an exchange of momentum, with momentum densities for photons and baryons given by (Hu & Sugiyama 1996):

$$(\rho_\gamma + p_\gamma)\, V_\gamma = \frac{4}{3}\rho_\gamma V_\gamma \qquad \text{for photons}$$
$$(\rho_b + p_b)\, V_b \simeq \rho_b V_b \qquad \text{for baryons}, \quad (10)$$

where V_γ and V_b are the photon and baryon bulk velocities. As a consequence of momentum conservation, the rate of change of the baryon velocity due to Compton drag is scaled by a factor of R_b^{-1} compared with the photon case, which means that (Hu & Sugiyama 1996)

$$\dot\tau_d = \frac{\dot\tau}{R_b} \quad (11)$$

where τ_b and τ are the Compton optical depths for baryons and photons respectively. Since the epoch of photon decoupling is defined by $\tau(z_*) = 1$, and the drag epoch is defined by $\tau_d(z_d) = 1$, $z_* = z_d$ only if $R_b = 1$. We live in a universe with a low baryon density, $R_b(z_*) < 1$ (see Eq.[8]), thus $\tau_d(z_d) = 1$ requires $z_d < z_*$, i.e., the drag epoch occurs *after* photon decoupling (Hu & Sugiyama 1996).

The redshift of the drag epoch z_d is well approximated by (Eisenstein & Hu 1998)

$$z_d = \frac{1291(\Omega_m h^2)^{0.251}}{1+0.659(\Omega_m h^2)^{0.828}} \left[1 + b_1 (\Omega_b h^2)^{b2}\right], \quad (12)$$

where

$$b_1 = 0.313(\Omega_m h^2)^{-0.419} \left[1 + 0.607(\Omega_m h^2)^{0.674}\right], \quad (13)$$
$$b_2 = 0.238(\Omega_m h^2)^{0.223}. \quad (14)$$

Using this fitting formula for z_d, Komatsu et al. (2009) found that from the WMAP 5 year observations

$$s \equiv r_s(z_d) = 153.3 \pm 2.0\,\mathrm{Mpc}, \qquad z_d = 1020.5 \pm 1.6 \quad (15)$$

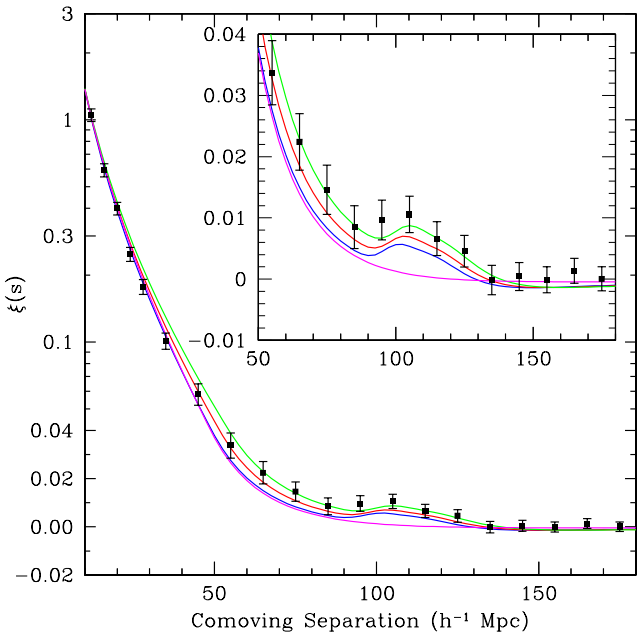

Figure 1. The large-scale redshift-space correlation function of the SDSS LRG sample measured by Eisenstein et al. (2005). The error bars are from the diagonal elements of the mock-catalog covariance matrix (the points are correlated). Note that the vertical axis mixes logarithmic and linear scalings. The inset shows an expanded view with a linear vertical axis. The models are $\Omega_m h^2 = 0.12$ (top), 0.13 (middle), and 0.14 (bottom), all with $\Omega_b h^2 = 0.024$ and $n = 0.98$ and with a mild non-linear prescription folded in. The featureless smooth line shows a pure CDM model ($\Omega_m h^2 = 0.105$), which lacks the acoustic peak. The bump at $100h^{-1}\,\mathrm{Mpc}$ scale is statistically significant.

2 BAO OBSERVATIONAL RESULTS

The power of BAO as a standard ruler resides in the fact that the BAO scale can in principle be measured in both radial and transverse directions, with the radial measurement giving $H(z)$ directly, and the transverse measurement giving $D_A(z)$. However, there are only a few published papers on measuring the BAO scale from the existing galaxy redshift survey data, and most of them extract a spherically averaged BAO scale (Eisenstein et al. 2005; Hutsi 2006; Percival et al. 2007).

Eisenstein et al. (2005) and Hutsi (2006) found roughly consistent spherically averaged correlation functions using SDSS data, with about the same BAO scale. Fig.1 shows the galaxy correlation function $\xi(s)$ measured from the SDSS data by Eisenstein et al. (2005). This BAO scale measurement is usually quoted in the form of

$$A_{BAO} \equiv \left[r^2(z_m)\,\frac{cz_m}{H(z_m)}\right]^{1/3} \frac{\left(\Omega_m H_0^2\right)^{1/2}}{cz_m}$$
$$= 0.469 \left(\frac{n_S}{0.98}\right)^{-0.35} \pm 0.017 \quad (16)$$

where $z_m = 0.35$, and n_S denotes the power-law index of the primordial matter power spectrum. Note that A_{BAO} essentially measures the product of a volume-averaged distance

$$d_V \propto \left[cH^{-1}(z)\, D_A(z)^2\right]^{1/3}, \quad (17)$$

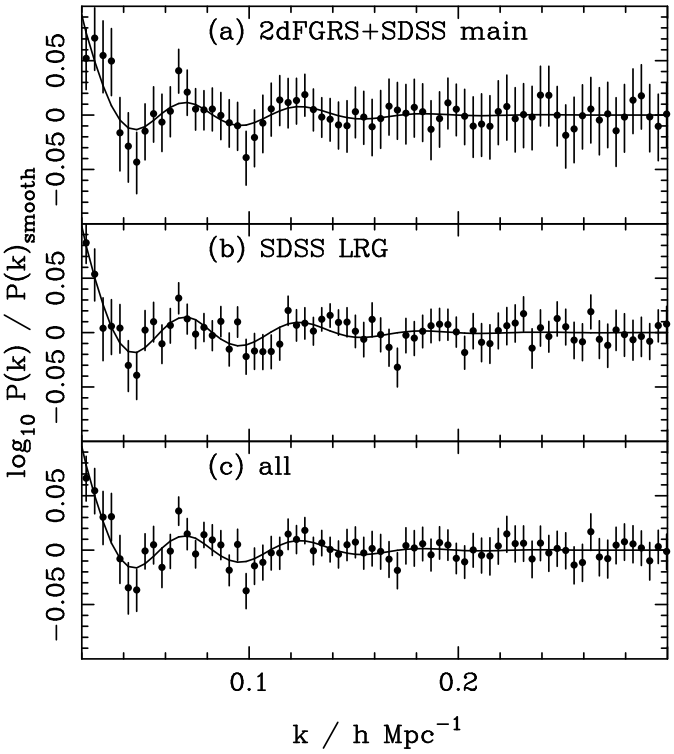

Figure 2. BAO in power spectra derived by Percival et al. (2007) from (a) the combined SDSS and 2dF main galaxies, (b) the SDSS DR5 LRG sample, and (c) the combination of these two samples. The data are correlated and the errors are calculated from the diagonal terms in the covariance matrix. A Standard ΛCDM distance–redshift relation was assumed to calculate the power spectra with $\Omega_m = 0.25$, $\Omega_\Lambda = 0.75$. The power spectra were then fitted with a cubic spline × BAO model, assuming the fiducial BAO model calculated using *CAMB*. The BAO component of the fit is shown by the solid line in each panel.

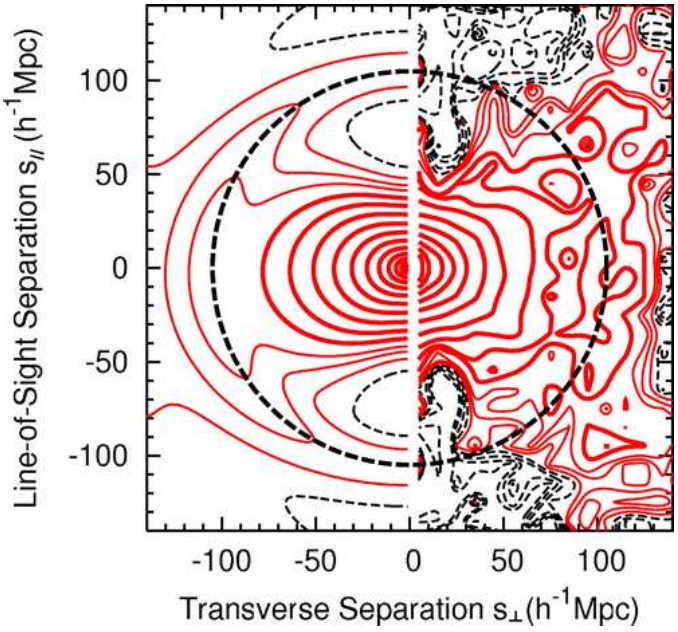

Figure 3. Contour plots of the redshift-space two-point correlation function measured from the SDSS LRG sample by Okumura et al. (2008). The right half of the figure shows their measurement, and the left half shows the corresponding analytical formula derived by Matsubara (2004) using a linear perturbation theory (Matsubara 2004). The thin dashed lines show $\xi < -0.01$ increasing logarithmically with increment 0.25 and $-0.01 \leqslant \xi < 0$ linearly with increment 0.0025. The solid thin lines show $0 \leqslant \xi < 0.01$ increasing linearly with increment 0.0025 and the solid thick lines $\xi \geqslant 0.01$ logarithmically with increment 0.25. The baryonic feature appears marginally as ridge structures around the scale $s = (s_\perp^2 + s_\parallel^2)^{1/2} \simeq 100\,h^{-1}$ Mpc, and the dashed circle traces the peaks of the baryon ridges.

multiplied by the square root of the matter density ($\rho_m(z) \propto \Omega_m h^2$). The one dimensional marginalized values are $\Omega_m h^2 = 0.130 \pm 0.010$, and $d_V(z_m) = 1370 \pm 64$ Mpc, assuming a fixed value of $\Omega_b h^2 = 0.024$ (Eisenstein et al. 2005). The product of $d_V(z_m)$ and $\Omega_m h^2$ is more tightly constrained than $d_V(z_m)$ or $\Omega_m h^2$ by the data, because the measured values of $d_V(z_m)$ and $\Omega_m h^2$ are correlated. Note that $A_{BAO} \propto d_V \cdot (\Omega_m h^2)^{1/2}$ is independent of the Hubble constant h, and its measured value is independent of a dark energy model (Eisenstein et al. 2005).

Clearly, the BAO constraint in Eq.(16) from Eisenstein et al. (2005) is not just a simple measurement of the BAO feature; it also relies on the constraints on $\Omega_m h^2$ from measuring the power spectrum turnover scale (related to matter-radiation equality). The latter makes the BAO constraint from Eisenstein et al. (2005) less robust than it would be otherwise. A new analysis of the SDSS data to derive truly robust and detailed BAO constraints would be very useful for placing dark energy constraints (Dick, Knox, & Chu 2006).

Percival et al. (2007) found that the power spectra from combined SDSS and 2dF data give spherically averaged BAO scales at $z = 0.2$ and $z = 0.35$ that are inconsistent with the prediction of the fiducial flat ΛCDM model at 2.4σ; this is in contradiction to the SN Ia data (which are consistent with the fiducial ΛCDM model at $z \lesssim 0.5$ at 1σ, see Riess et al. (2007)). Percival et al. (2007) found a similar discrepancy between SDSS main and SDSS LRG samples. Fig.2 shows BAO in power spectra calculated from (a) the combined SDSS and 2dF main galaxies, (b) the SDSS DR5 LRG sample, and (c) the combination of these two samples. The data are solid symbols with 1σ errors calculated from the diagonal terms in the covariance matrix.

The efforts to extract the BAO scale in both radial and transverse directions have led to contradicting results. Fig.3 shows the contour plots of the redshift-space two-point correlation function measured from a SDSS LRG sample (similar to DR3) by Okumura et al. (2008). The baryonic feature appears marginally as ridge structures around the scale $s = (s_\perp^2 + s_\parallel^2)^{1/2} \simeq 100\,h^{-1}$ Mpc, and the dashed circle traces the peaks of the baryon ridges. Okumura et al. (2008) found that current galaxy redshift survey data are not adequate for extracting the BAO scale in both radial and transverse directions to measure $H(z)$ and $D_A(z)$. However, an independent analysis by Gaztanaga, Cabre, & Hui (2008) found that $H(z)$ can be measured quite accurately from the SDSS DR6 data, with $H(z = 0.24) = 79.7 \pm 2.1(\pm 1.0)\,\mathrm{km\,s^{-1}Mpc^{-1}}$ for $z = 0.15$-0.30, and $H(z = 0.43) = 86.5 \pm 2.5(\pm 1.0)\,\mathrm{km\,s^{-1}Mpc^{-1}}$ for $z = 0.40$-0.47. The difference between the results of Okumura et al. (2008) and Gaztanaga, Cabre, & Hui (2008) cannot be explained by the statistics of the data used (DR3 versus DR6).

Resolving the dramatic discrepancy between Okumura et al. (2008) and Gaztanaga, Cabre, & Hui (2008) in the analysis of the radial and transverse BAO scales is of critical importance to the understanding of BAO systematics, and the accurate forecasting of the capabilities of planned future galaxy redshift surveys. All current forecasts of future surveys assume that both radial and transverse BAO scales can be accurately extracted, and use either the

Fisher matrix formalism (which gives the smallest possible errors) or methods based on numerical simulations that are not yet fully validated by application to real data.

Recently, Chuang & Wang (2012a) made the first simultaneous measurements of $H(z)$ and $D_A(z)$ from galaxy redshift survey data. They validated their method using LasDamas mock galaxy catalogs. Applying their method to the sample of SDSS DR7 LRGs, they obtained $H(z = 0.35) \equiv H(0.35) = 82.1^{+4.8}_{-4.9}\mathrm{km\,s^{-1}Mpc^{-1}}$, $D_A(z = 0.35) \equiv D_A(0.35) = 1048^{+60}_{-58}$ Mpc without assuming a dark energy model or a flat Universe. They found that the derived measurements of $H(0.35)\,r_s(z_d)$ and $D_A(0.35)/r_s(z_d)$ (where $r_s(z_d)$ is the sound horizon at the drag epoch) are nearly uncorrelated, have tighter constraints and are more robust with respect to possible systematic effects. Their galaxy clustering measurements of $\{H(0.35)\,r_s(z_d)/c, D_A(0.35)/r_s(z_d)\} = \{0.0434 \pm 0.0018, 6.60 \pm 0.26\}$ (with the correlation coefficient $r = 0.0604$) can be used to combine with cosmic microwave background and any other cosmological data sets to constrain dark energy. This work has significant implications for future surveys in establishing the feasibility of measuring both $H(z)$ and $D_A(z)$ from galaxy clustering data.

Fig.4 shows the 2D 2PCF measured from the SDSS LRGs and a single LasDamas SDSS LRG mock catalog for comparison (Chuang & Wang 2012a). The similarity between the data and the mock in the range of scales used (indicated by the shaded disk) is apparent. Due to the current limitations in the modeling of systematic effects, only the quasi-linear scale range of $s = 40 - 120\,h^{-1}$Mpc is used for a conservative estimate in this analysis.

Very recently, Reid et al. (2012) measured $H(z)$, $D_A(z)$, and growth constraints at $z = 0.57$ from the monopole and quadrupole of the 2D 2PCF of the SDSS III Baryon Oscillation Spectroscopic Survey (BOSS) (SDSS DR9) sample of galaxies, assuming CMB priors. Most recently, Xu et al. (2012) measured $H(z)$ and $D_A(z)$ at $z = 0.35$ from the SDSS DR7 LRGs by applying density-field reconstruction to an anisotropic analysis of the BAO peak (see Sec.3.1 for a description of this technique).

Overall, we have made dramatic progress within the last two years toward developing robust methods to fully analyze the data from current and planned future galaxy redshift surveys.

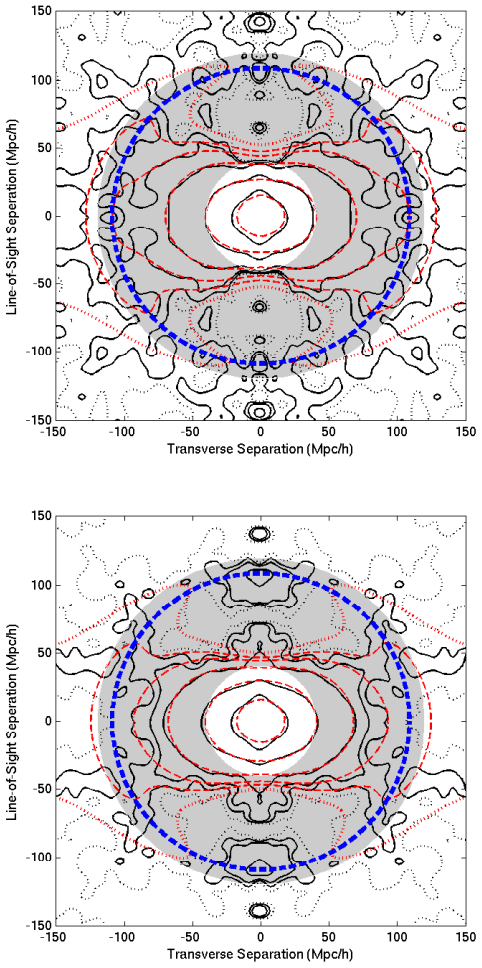

Figure 4. The two-dimensional two-point correlation function (2D 2PCF) measured from SDSS DR7 LRGs (top panel) and a LasDamas SDSS LRG mock catalog (bottom panel) in a redshift range $0.16 < z < 0.44$ (solid black contours), compared to a theoretical correlation function with parameters close to the best fit values in the likelihood analysis (dashed red contours). In both figures, the shaded disk indicates the scale range considered ($s = 40 - 120\ h^{-1}$Mpc) in this study. The thick dashed blue circle denotes the baryon acoustic oscillation scale. The observed 2D 2PCF has been smoothed by a Gaussian filter with rms variance of $2h^{-1}$Mpc for illustration in these figures only; smoothing is not used in our likelihood analysis. The contour levels are $\xi = 0.5, 0.1, 0.025, 0.01, 0.005, 0$. The $\xi = 0$ contours are denoted with dotted lines for clarity. (Chuang & Wang 2012a)

3 BAO SYSTEMATIC EFFECTS

The systematic effects of BAO as a standard ruler are: bias between galaxy and matter distributions, nonlinear effects, and redshift-space distortions (Blake & Glazebrook 2003; Seo & Eisenstein 2003). Cosmological N-body simulations are required to quantify these effects (Angulo et al. 2005; Seo & Eisenstein 2005; Springel et al. 2005; White 2005; Jeong & Komatsu 2006; Koehler, Schuecker, & Gebhardt 2007; Angulo et al. 2008).

To be specific in our discussion on the systematic effects in the BAO scale measurement, we will use the results from Angulo et al. (2008) to illustrate. All the results from Angulo et al. (2008) shown here are from a numerical simulation covering a comoving cube volume of side $1340\,h^{-1}$ Mpc, in which dark matter is represented by more than 3 billion particles (1448^3), with the particle mass of $5.49\times10^{10}\ h^{-1}\,\mathrm{M}_\odot$. This simulation corresponds to a comoving volume of $2.41\,h^{-3}$ Gpc^3, more than three times the volume of the catalog of SDSS LRGs used in the BAO detection by Eisenstein et al. (2005). It assumes a ΛCDM model with $\Omega_m = 0.25$, $\Omega_\Lambda = 0.75$, $\sigma_8 = 0.9$, and $h = H_0/(100\,\mathrm{km\,s^{-1}Mpc^{-1}})$=0.73.

In the current picture of structure formation in the universe, primordial matter density perturbations (which are responsible for the observed CMB anisotropy) seeded the cosmic large scale structure. Matter density fluctuations grew with time. Dense regions became denser, and galaxy clusters and galaxy haloes formed first in such regions. Galaxy formation (in which baryons played a critical part) occurred in galaxy haloes.

Since we have to use galaxies to trace the matter density field, it is important for a numerical simulation to assign galaxies properly. Angulo et al. (2008) used a semi-analytic model to describe the key physical processes which are thought to determine the for-

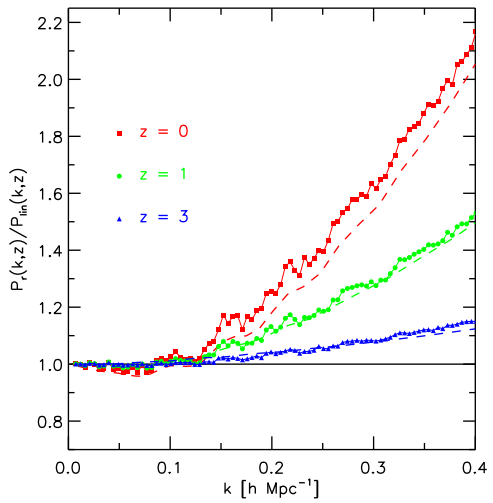

Figure 5. The nonlinear growth of the matter power spectrum (Angulo et al. 2008). The power spectrum in real-space (measured at the redshift indicated by the key) is divided by the power spectrum at $z = 15$, after taking into account the change in the growth factor. Any deviation of the resulting ratio from unity indicates a departure from linear perturbation theory. The dashed lines show the same ratio as predicted using the ansatz of Smith et al. (2003) which transforms the linear power spectrum into the nonlinear power spectrum (Smith et al. 2003). The simulation corresponds to a comoving volume of 2.41 h^{-3} Gpc^3.

mation and evolution of galaxies; this approach mirrors the hybrid schemes introduced by Kauffmann, Nusser, & Steinmetz (1997) and Benson e tal. (2000). This model makes an *ab initio* prediction of which dark matter haloes should contain galaxies by modeling the physics of the baryonic component of the universe (Baugh et al. 2005; Baugh 2006). The specific model used by Angulo et al. (2008) reproduces the abundance of Lyman-break galaxies at $z = 3$ and $z = 4$, and the number counts of sub-mm detected galaxies (with a median redshift $z \sim 2$). It also gives a rough match to the abundance of luminous red galaxies (Almeida et al. 2008), and a reasonable match to the observed properties of local galaxies (e.g. Nagashima et al. (2005b,a); Almeida, Baugh, & Lacey (2007)).

3.1 Nonlinear effects

On very large scale, the growth of density perturbations is linear, and the different comoving wavelength scales are not coupled. When the amplitude of density perturbations on a given scale reaches order unity, nonlinear growth occurs, i.e., the evolution of the different wavelength modes becomes increasingly coupled, leading to a departure from linear evolution. Thus nonlinear effects erase the BAO in the matter power spectrum on small scales, distort the matter power spectrum on quasi-linear scales, and degrade the BAO signal on linear scales. The characteristic comoving scale for nonlinearity increases with cosmic time, as density perturbations on larger and larger comoving scales grow to be of order unity in amplitude. Fig.5 shows the nonlinear growth of the matter power spectrum measured from a numerical simulation by Angulo et al. (2008). Nonlinear effects have to be removed or corrected for in the data analysis in order to obtain robust BAO scale measurements (see for example, Refs.(Jeong & Komatsu 2006; Koehler, Schuecker, & Gebhardt 2007; Smith, Scoccimarro, & Sheth 2007; Crocce & Scoccimarro 2008)).

The most troublesome consequence of nonlinear effects is the shift in the observed BAO scale in galaxy redshift survey data from the CMB-calibrated prediction. It is most intuitive to consider this effect in real space, where the nonlinear growth of density perturbations damps and shifts the BAO peak at $\sim 100h^{-1}$ Mpc, because the large-scale bulk flows cause the differential motions of the galaxy pairs initially separated by the sound horizon scale at the drag epoch (Eisenstein et al. 2007).

Eisenstein et al. (2007); Seo et al. (2008) introduced a method to "reconstruct" the linear power spectrum from a nonlinearly evolved galaxy distribution in order to minimize the impact of nonlinear effects on the constraining power of BAO as a dark energy probe. They found that the shifts of the BAO peak can be predicted numerically, and can be substantially reduced (to less than 0.1% at $z = 0.3 - 1.5$) using a simple "density-field reconstruction" method (Eisenstein et al. 2007; Seo et al. 2008).

Padmanabhan, White, Cohn (2009) reformulated this reconstruction method within the Lagrangian picture of structure formation, and found that this reconstruction does *not* reproduce the linear density field, at second order. They showed that it does reduce the damping of the BAO due to non-linear structure formation. In particular, they showed that reconstruction reduces the mode-coupling term in the power spectrum, thus reducing the bias in the estimated BAO scale when the reconstructed power spectrum is used. Note that the reconstruction technique has only been demonstrated for dark matter, and not yet for haloes or galaxies.

3.2 Redshift-space distortions

Redshift-space distortions are the consequence of peculiar motions on the measurement of the power spectrum from a galaxy redshift survey. Peculiar motions produce different types of distortion to the power spectrum. On large scales, coherent bulk flows out of voids and into overdense regions lead to an enhancement in the density inferred in redshift-space, and hence to a boost in the recovered power. On small scales, the random motions of objects inside virialized dark matter haloes cause structures to appear elongated when viewed in redshift-space ("the finger of God" effect), leading to a damping of the power.

The enhancement of the power spectrum due to redshift-space distortions, under the assumption of linear perturbation theory for an observer situated at infinity (the plane parallel approximation), is given by (Kaiser 1987):

$$\frac{P_{\rm s}(k,\mu)}{P_{\rm r}(k,\mu)} = \left(1+\beta\mu^2\right)^2, \qquad (18)$$

where $P_{\rm s}(k,\mu)$ is the power spectrum in redshift-space, $P_{\rm r}(k,\mu)$ is the power spectrum in real-space, and $\mu = \mathbf{k}\cdot\hat{\mathbf{r}}/k$, with $\hat{\mathbf{r}}$ denoting the unit vector along the line of sight. The redshift-space distortion parameter β is defined as

$$\beta(z) \equiv \frac{f_g(z)}{b(z)}, \qquad (19)$$

where $f_g(z)$ denotes the growth rate, and $b(z)$ denotes the bias factor. Eq.(18) can be derived using

$$\frac{d\delta}{dt} = -\boldsymbol{\nabla}\cdot\delta\mathbf{v}, \qquad (20)$$

where δ is the matter density perturbation, and $\delta\mathbf{v}$ is the peculiar velocity, and requiring that the number of galaxies is conserved when we go from real to redshift space (Hamilton 1998).

The enhancement of the spherically averaged power spectrum is

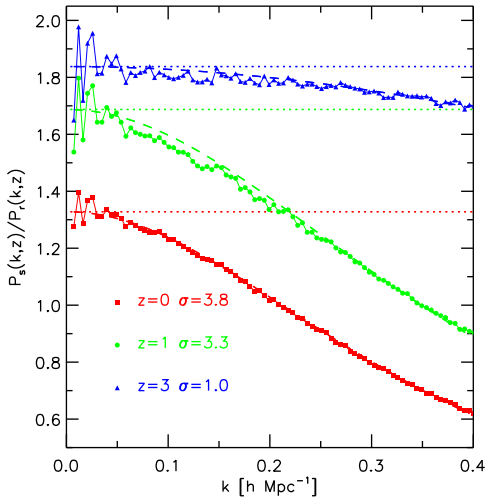

Figure 6. The ratio of the power spectrum measured for the dark matter in redshift-space, i.e. including the impact of peculiar motions in the distance determination, to the power spectrum measured in real-space (Angulo et al. 2008). The deviation from unity shows the redshift-space distortion to the nonlinear power spectrum. The results are shown for selected output redshifts, as indicated by the key. The horizontal dotted lines indicate the boost in the redshift-space power expected due to coherent flows, as predicted by Eq.(21). The dashed lines show a simple fit to the distortions (see Eq.[22]). The simulation corresponds to a comoving volume of 2.41 h^{-3} Gpc^3.

$$\frac{P_{\rm s}(k)}{P_{\rm r}(k)} = 1 + \frac{2}{3}\beta + \frac{1}{5}\beta^2, \tag{21}$$

which follows from integration over μ.

Eq.(21) can be modified to include the damping effect due to the "the finger of God" effect (Angulo et al. 2008):

$$\frac{P_{\rm s}(k)}{P_{\rm r}(k)} = \frac{1 + \frac{2}{3}\beta + \frac{1}{5}\beta^2}{1 + k^2\sigma^2}, \tag{22}$$

where σ is a free parameter associated with the pairwise velocity dispersion, see Eq.(105).

Fig.6 shows the ratio of the matter power spectrum measured in redshift-space, to the matter power spectrum measured in real-space (Angulo et al. 2008). Clearly, Eq.(22) provides a good description for redshift-space distortion to the matter power spectrum.

Since we cannot directly measure the matter power spectrum, we have to study the redshift-space distortion to the power spectrum of the type of object used as matter tracer in the galaxy redshift survey. The form of the redshift-space distortion to the power spectrum depends on the type of object under consideration.

In current theories of galaxy formation, dark matter haloes are hosts to galaxies. Angulo et al. (2008) found that Eq.(22) is a poor description of the redshift-space distortions to the dark matter halo power spectrum, but is a reasonable description of the redshift-space distortions to the galaxy power spectrum.

The small-scale redshift-space distortions ("the finger of God" effect) can be removed from data in the BAO measurement using a nonlinear "finger-of-God" compression step *before* the power spectrum analysis, in which a "friends-of-friends" algorithm is used to identify the clustering of matter (Tegmark et al. 2004). However, this may introduce a degree of arbitrariness in the results. We can use the version of Eq.(22) before spherical averaging and its counter part in the correlation function analysis to fully model both the large-scale compression and the small-scale "finger of God" effect due to redshift-space distortions.

Note that the redshift-space distortions on large scales do not modify the BAO, and can be used to measure the linear redshift-space distortion parameter β.

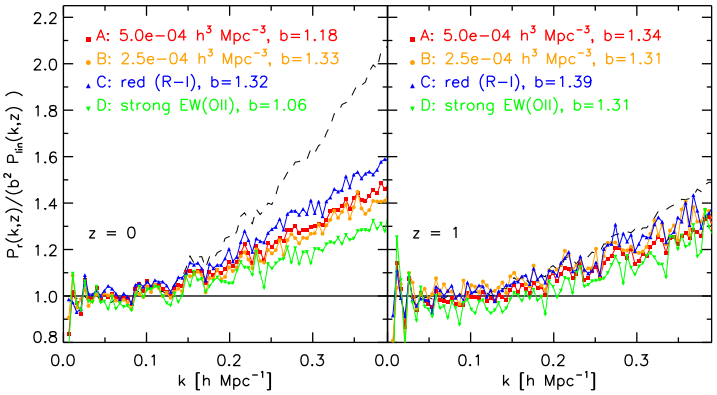

Figure 7. The power spectrum of different galaxy samples measured in real-space, divided by the square of an effective bias parameter and the appropriately scaled linear perturbation theory power spectrum (Angulo et al. 2008). The sample definition and the value of the effective bias used are given by the key. The power spectrum of the dark matter spectrum in real-space, also divided by the linear perturbation theory spectrum, is shown by the dashed line. The left hand panel shows the ratios at $z = 0$ and the right hand panel at $z = 1$. The simulation corresponds to a comoving volume of 2.41 h^{-3} Gpc^3.

3.3 Scale-dependent bias

The bias factor between the tracer distribution measured by the galaxy redshift survey and the matter distribution depends on the tracer used. Angulo et al. (2008) showed that the clustering of haloes is *not* a shifted version of that of the dark matter, in contrast to current theoretical models. The bias between dark matter haloes and dark matter is scale-dependent, and the variation in the degree of scale-dependence with redshift is not monotonic. The scale-dependence of the bias for galaxies is less than that of dark matter haloes, but still significant (Angulo et al. 2008).

Fig.7 shows the real space power spectrum for four different samples of galaxies, divided by the square of an effective bias parameter and the appropriately scaled linear perturbation theory power spectrum. Samples A and B denote galaxies from an R-magnitude limited survey with a given space density. Sample C contains the reddest 50% of galaxies from sample A (selected using the $R-I$ color). Sample D contains the 50% of galaxies from sample A with the strongest emission lines, selected using the equivalent width of OII[3727]. The dashed line shows the real-space power spectrum of matter divided by the appropriate linear perturbation theory power spectrum.

Note that since nonlinear effects are independent of the galaxy sample, the differences in the power spectra of the four different galaxy samples in Fig.7 indicate that bias depends strongly on the galaxy sample, and that bias is scale-dependent. Therefore, scale-dependent bias must be properly modeled if quasi-linear scales are included in the analysis of BAO scales.

4 BAO DATA ANALYSIS TECHNIQUES

We will discuss two approaches to probing the BAO, using the galaxy power spectrum (Sec.4.1) and using galaxy two-point correlation function (Sec.4.2). In both methods, the actual galaxy distribution is compared with a catalog of randomly distributed galaxies. These randomly distributed galaxies have the same redshift, magnitude, and mask constraints as the real data.

The BAO scales extracted from the two different analysis methods provide an important cross-check. We will discuss the potential of each method for mitigating systematic effects.

A way to test how well we can extract the BAO scale from real data is to apply the two analysis techniques to simulated data. To measure the power spectrum or correlation function of galaxies, one must convert the angular positions and redshifts of the galaxies into comoving spatial separations. This requires assuming a set of values of the cosmological parameters, including the dark energy parameters. The effect of a change in the value of dark energy parameters is to change the separations between pairs of galaxies, which leads to a change in the appearance of the galaxy power spectrum and correlation function. For small perturbations away from the true dark energy parameters, one can assume that the change in the measured galaxy power spectrum and correlation function can be represented by a rescaling of the wavenumber from $k_{\rm true}$ to $k_{\rm app}$ for the power spectrum, and a rescaling of the length scale from $r_{\rm true}$ to $r_{\rm app}$ for the correlation function. For simplicity, we will focus on spherically averaged data. The *scale parameter*, α, describes the change in the recovered BAO scale:

$$\begin{aligned} \alpha &= \frac{k_{\rm app}}{k_{\rm true}} \quad \text{power spectrum;} \\ \alpha &= \frac{r_{\rm true}}{r_{\rm app}} \quad \text{correlation function.} \end{aligned} \tag{23}$$

If dark energy parameter are estimated correctly, then there is no shift in the BAO in the estimated power spectrum and $\alpha = 1$. In the case of a wide-angle, deep galaxy survey with spectroscopic redshifts, the stretch parameter can be approximated by (Angulo et al. 2008):

$$\alpha \approx \left(\frac{D_A(z, X_{\rm assumed})}{D_A(z, X_{\rm true})}\right)^{-2/3} \left(\frac{H(z, X_{\rm assumed})}{H(z, X_{\rm true})}\right)^{1/3}, \tag{24}$$

where $X(z) = \rho_X(z)/\rho_X(0)$ denotes the dark energy density function.

The accuracy and precision of the BAO scale measurement is reflected by that of the scale parameter α. This in turn depends on the modeling of the BAO in the data analysis. A common misconception is that the location of the BAO peaks in the galaxy power spectrum or two-point correlation function corresponds *exactly* to the sound horizon scale at the drag epoch. This misconception can lead to biased estimate of the BAO scale and hence biased estimate of cosmological and dark energy parameters. To accurately extract the BAO scale, the galaxy power spectrum and two-point correlation function must be modeled as completely as possible.

4.1 Using the galaxy power spectrum to probe BAO

The real space galaxy power spectrum is related to the matter power spectrum as follows:

$$P_g(k, z) = b(z) P_m(k, z), \tag{25}$$

where $b(z)$ is the bias factor between galaxy and matter distributions.

The matter power spectrum

The matter power spectrum is defined as

$$P_m(k) \equiv \left|\delta_{\mathbf{k}}\right|^2 \tag{26}$$

where $\delta_{\mathbf{k}}$ is the Fourier transform of the matter density perturbation $\delta(\mathbf{r})$, defined as

$$\delta_{\mathbf{k}} \equiv \int \delta(\mathbf{r})\, e^{i\mathbf{k}\cdot\mathbf{r}}\, {\rm d}^3\mathbf{r}. \tag{27}$$

Therefore

$$\delta(\mathbf{r}) \equiv \frac{\rho(\mathbf{r}) - \bar{\rho}}{\bar{\rho}} = \frac{1}{(2\pi)^3} \int \delta_{\mathbf{k}}\, e^{-i\mathbf{k}\cdot\mathbf{r}}\, {\rm d}^3\mathbf{k}, \tag{28}$$

with $\rho(\mathbf{r})$ and $\bar{\rho}(\mathbf{r})$ denoting the matter density at position $\mathbf{r}$ and the mean matter density respectively. Note that

$$\int e^{i\mathbf{k}\cdot\mathbf{r}}\, {\rm d}^3\mathbf{r} = (2\pi)^3 \delta^D(\mathbf{k}), \tag{29}$$

where δ^D denotes the Dirac delta function.

The theoretical matter power spectrum in the linear regime is given by

$$P(k)_{lin} = P_0\, k\, A_s^2(k) T^2(k), \tag{30}$$

where P_0 is a normalization constant, $A_s^2(k)$ is the power spectrum of primordial matter density fluctuations, and $T(k)$ is the matter transfer function. The primordial power spectrum is determined by unknown inflationary physics in the very early universe, and can be measured directly from data in a model-independent manner (Wang, Spergel, & Strauss 1999; Mukherjee & Wang 2003). For simplicity, the primordial matter power spectrum is usually parametrized as a power-law:

$$k\, A_s^2(k) \propto k^{n_S}. \tag{31}$$

The matter transfer function $T(k)$ describes how the evolution of matter density perturbations depends on scale.

In the inflationary paradigm of the very early universe, density perturbations began as quantum fluctuations produced during inflation within the horizon for microphysics, the Hubble radius $H(t)^{-1}$ (where $H(t)$ is the Hubble parameter). The Hubble radius remained roughly constant during inflation, while the universe underwent extremely rapid expansion, stretching the physical scales of density perturbations ($\lambda_{phys} \propto a(t)\lambda$ for a comoving wavelength λ). Thus density perturbations crossed outside the microphysics horizon during inflation. After inflation, the universe was radiation dominated (with $a(t) \propto t^{1/2}$), then became matter dominated (with $a(t) \propto t^{2/3}$) after the matter-radiation equality epoch z_{eq} (see Eq.[5]). The Hubble radius grew faster than the cosmic scale factor $a(t)$ during both radiation and matter domination, since $H^{-1}(t) = [\dot{a}/a]^{-1} \propto t$. Thus density perturbations re-entered the microphysics horizon after inflation; those that exited the microphysics horizon last during inflation (the smallest scales) re-entered first. Since matter density perturbations could not grow until the universe became matter dominated, the growth of matter density perturbations is scale-dependent. This is encoded in the matter transfer function T(k), and depends on the physics at matter-radiation equality and photon-decoupling. If dark energy perturbations are negligible, $T(k)$ only depends on the matter density $\rho_m \propto \Omega_m h^2$ and baryon density $\rho_b \propto \Omega_b h^2$, and on the dimensionless Hubble constant h through the choice of h/Mpc as the

unit for k. It is most convenient and reliable to calculate $T(k)$, normalized such that $T(k \to 0) = 1$, using a public high precision CMB code such as *CMBFAST* (Seljak & Zaldarriaga 1996) or *CAMB* (Lewis, Challinor, & Lasenby 2000).

The galaxy power spectrum can be measured from data using the FKP method (Feldman, Kaiser, & Peacock 1994). This method uses galaxy catalogs obtained from galaxy surveys and a much larger synthetic galaxy catalog with the same angular and radial selection functions.

Basic idea behind the FKP method for estimating $P_g(k)$

It is the locations of galaxies, and not the smooth matter density field $\rho(\mathbf{r})$ that is observed. The basic idea behind the FKP method is to take the Fourier transform of the distribution of real galaxies, minus the transform of a synthetic catalog with the same angular and radial selection function as the real galaxies but otherwise without structure. It also incorporates a weight function $w(\mathbf{r})$ which is adjusted to optimize the performance of the power-spectrum estimator. It defines a weighted galaxy fluctuation field, with a convenient normalization, to be

$$F(\mathbf{r}) \equiv \frac{w(\mathbf{r})\left[n_g(\mathbf{r}) - \alpha_s n_s(\mathbf{r})\right]}{\left[\int d^3r\, \overline{n}^2(\mathbf{r})\, w^2(\mathbf{r})\right]^{1/2}}, \tag{32}$$

where $\overline{n}(\mathbf{r})$ is the expected mean space density of galaxies given the angular and luminosity selection criteria, and

$$n_g(\mathbf{r}) = \sum_i \delta^D(\mathbf{r} - \mathbf{r}_i^g), \qquad n_s(\mathbf{r}) = \sum_i \delta^D(\mathbf{r} - \mathbf{r}_i^s) \tag{33}$$

with $\mathbf{r}_i$ denoting the location of the $i^{\rm th}$ galaxy from the real (with superscript "g") or synthetic (with superscript "s") catalog. The synthetic catalog has a number density that is $1/\alpha_s$ times that of the real catalog. The synthetic catalog is created assuming that galaxies form a Poisson sample of the density field, $\rho/\bar{\rho}$ (Peebles 1980).

Denoting the Fourier transform of $F(\mathbf{r})$ as $F(\mathbf{k})$, it can be shown that

$$\begin{aligned} \langle|F(\mathbf{k})|^2\rangle &= \int \frac{d^3k'}{(2\pi)^3} P_g(\mathbf{k}')|G(\mathbf{k}-\mathbf{k}')|^2 + \\ (1+\alpha_s) & \quad \frac{\int d^3r\, \overline{n}(\mathbf{r})\, w^2(\mathbf{r})}{\int d^3r\, \overline{n}^2(\mathbf{r})\, w^2(\mathbf{r})} \end{aligned} \tag{34}$$

where the window function

$$G(\mathbf{k}) \equiv \frac{\int d^3r\, \overline{n}(\mathbf{r})\, w(\mathbf{r})\, e^{i\mathbf{k}\cdot\mathbf{r}}}{\left[\int d^3r\, \overline{n}^2(\mathbf{r})\, w^2(\mathbf{r})\right]^{1/2}}. \tag{35}$$

For a typical galaxy redshift survey, $G(\mathbf{k})$ is a compact function with width $\sim 1/D$, where D characterizes the depth of the survey. Assuming that we have a "fair sample" of the matter density distribution, then

$$\langle|F(\mathbf{k})|^2\rangle \simeq P_g(\mathbf{k}) + P_{\rm shot}, \tag{36}$$

where the constant shot noise component

$$P_{\rm shot} \equiv \frac{(1+\alpha_s)\int d^3r\, \overline{n}(\mathbf{r})\, w^2(\mathbf{r})}{\int d^3r\, \overline{n}^2(\mathbf{r})\, w^2(\mathbf{r})}. \tag{37}$$

The FKP estimator of $P_g(\mathbf{k})$ is thus

$$\hat{P}_g(\mathbf{k}) = |F(\mathbf{k})|^2 - P_{\rm shot}, \tag{38}$$

with the final estimator of $P_g(k)$ given by averaging $\hat{P}_g(\mathbf{k})$ over a shell in k-space:

$$\hat{P}_g(k) \equiv \frac{1}{V_k}\int_{V_k} d^3k'\, \hat{P}_g(\mathbf{k}'), \tag{39}$$

where V_k is the volume of the shell.

Practical implementation of the FKP method for estimating $P_g(k)$

The radially averaged power spectrum from the FKP estimator is

$$\hat{P}_g(k) = \frac{1}{N_k}\sum_{k<|\mathbf{k}|<k+\delta k}\left[|F(\mathbf{k})|^2 - S(0)\right] \tag{40}$$

where N_k is the number of modes in the shell, and $F(\mathbf{k})$ and $S(\mathbf{k})$ are given by

$$\begin{aligned} F(\mathbf{k}) &= \int d^3r\; w(\mathbf{r})[n_g(\mathbf{r}) - \alpha_s n_s(\mathbf{r})]e^{i\mathbf{k}\cdot\mathbf{r}} \\ &\to \sum_g w(\mathbf{r}_g)e^{i\mathbf{k}\cdot\mathbf{r}_g} - \alpha_s\sum_s w(\mathbf{r}_s)e^{i\mathbf{k}\cdot\mathbf{r}_s}, \\ S(\mathbf{k}) &= (1+\alpha_s)\int d^3r\, \overline{n}(\mathbf{r})\, w^2(\mathbf{r})\, e^{i\mathbf{k}\cdot\mathbf{r}} \\ &\to \alpha_s(1+\alpha_s)\sum_s w^2(\mathbf{r}_s)e^{i\mathbf{k}\cdot\mathbf{r}_s}. \end{aligned} \tag{41}$$

Note that for convenience, we have adjusted the normalization of the weight function so that

$$\int d^3r\, \overline{n}^2(\mathbf{r})\, w^2(\mathbf{r}) \to \alpha_s\sum_s \overline{n}(\mathbf{r}_s)\, w^2(\mathbf{r}_s) = 1 \tag{42}$$

The variance of the estimated $P(k)$, for any shell thickness, is

$$\sigma_P^2(k) = \frac{2}{N_k^2}\sum_{\mathbf{k}'}\sum_{\mathbf{k}''}\left|P_g Q(\mathbf{k}'-\mathbf{k}'') + S(\mathbf{k}'-\mathbf{k}'')\right|^2 \tag{43}$$

where $\mathbf{k}$ and $\mathbf{k}'$ are constrained to lie in the shell, and

$$Q(\mathbf{k}) = \int d^3r\, \overline{n}^2(\mathbf{r})\, w^2(\mathbf{r})\, e^{i\mathbf{k}\cdot\mathbf{r}} \to \alpha_s\sum_s \overline{n}(\mathbf{r}_s)\, w^2(\mathbf{r}_s)e^{i\mathbf{k}\cdot\mathbf{r}_s}. \tag{44}$$

The weight function $w(\mathbf{r})$ is chosen such that it minimizes the variance $\sigma_P^2(k)$. This leads to

$$w(\mathbf{r}) = \frac{1}{1+\overline{n}(\mathbf{r})P_g(k)}. \tag{45}$$

Note that the weight function depends on the assumed value for $P_g(k)$. The optimal estimator results from allowing a range of $P_g(k)$ and then selecting an optimal value for $P_g(k)$.

If the shell intercepts a sufficiently large number of coherent volumes, then the fractional error in the estimated $P_g(k)$ is reasonably small. Then the fluctuations in the power will become Gaussian distributed, and the likelihood for any particular theory represented by $P_{\rm g,th}(k)$ is

$$\begin{aligned} & L[P_{\rm g,th}(k)] \\ = \;& p[P_i|P_{\rm g,th}(k)] \\ = \;& \frac{1}{(2\pi)^{N/2}|C|}\exp\left\{-\frac{C_{ij}^{-1}}{2}[\hat{P}_{g,i} - P_{\rm g,th}(k_i)][\hat{P}_{g,j} - P_{\rm g,th}(k_j)]\right\}, \end{aligned} \tag{46}$$

where $\hat{P}_{g,i}$ is the vector of estimates, and the correlation matrix for the binned estimates of $\hat{P}_g$ is

$$\begin{aligned} C_{ij} &\equiv \langle\delta\hat{P}_g(k_i)\delta\hat{P}_g(k_j)\rangle \\ &= \frac{2}{N_k N_{k'}}\sum_{\mathbf{k}}\sum_{\mathbf{k}'}|P_g Q(\mathbf{k}-\mathbf{k}') + S(\mathbf{k}-\mathbf{k}')|^2 \end{aligned} \tag{47}$$

where $\mathbf{k}$ and $\mathbf{k}'$ lie in the shells around k_i and k_j respectively. Note that C_{ij} depends on $P_g(k)$.

The original FKP technique is a direct Fourier method; one first chooses a k grid with sufficient grid size and spacing and then obtain the Fourier transform by performing direct summation at each grid point (see Eqs.[40] and [41]), instead of using fast Fourier transform (FFT). However, it is possible to modify this method so that one can use FFT (for example, see Cole et al. (2005)). Unlike in the direct Fourier method, one has to assign galaxies to a linearly spaced grid using an interpolation method such as cloud in cell, nearest grid point, or triangular shaped cloud assignment scheme (Hockney & Eastwood 1998). This induces gridding noise and one needs to correct the resultant power spectrum for this. However, the direct Fourier method is much slower than the FFT method. In both methods, the final step involves obtaining power in thin spherical shells in k space to get the power spectrum. This resultant power spectrum is convolved with the window function of the survey as these surveys are volume limited. Therefore, one needs to deconvolve the obtained power spectrum with the window function of the survey. In practice, it is much more convenient to convolve the theoretical power spectrum with the survey window function, and compare it with the measured power spectrum (without deconvolution).

The power spectra for combined 2dF and SDSS data shown in Fig.2 were estimated by Percival et al. (2007) using a modified version of the FKP method, such that FFT is used instead of direct summation at each grid point. Note that the BAO signature can be seen clearly. However, there is a clear difference between the BAO scale present in the combined 2dF and SDSS main data and the BAO scale apparent in the SDSS LRG data.

Mitigation of systematic effects in BAO scale extraction from $P_g(k)$

Simulated data must be used to study how the BAO scale extraction from the measured galaxy power spectrum is affected by systematic effects. The BAO scale can be extracted by fitting the measured galaxy power spectrum to the linear perturbation theory power spectrum with appropriate modifications to allow for our ignorance on dark energy parameters and to model nonlinear effects. A simple method to model power spectrum data consists of the following steps (Percival et al. 2007; Angulo et al. 2008):

1. Construct a smooth reference spectrum $P_{\rm g,ref}$ from the measured galaxy power spectrum. $P_{\rm g,ref}$ results from a coarse rebinning of the measured power spectrum that erases any oscillatory features such as BAO. For example, one can use a cubic spline fit over the wavenumber range $0.0046 < (k/h\,{\rm Mpc}^{-1}) < 1.2$, using the measured spectrum smoothed over 25 bins in wavenumber (Angulo et al. 2008). The spline is constrained to pass through the data points.

2. Compute the ratio, R(k), of the measured galaxy power spectrum, $P_g(k)$, to the reference power spectrum, $P_{\rm g,ref}(k)$:

$$R(k) = \frac{P_g(k)}{P_{\rm g,ref}(k)}. \tag{48}$$

3. Generate a linear perturbation theory matter power spectrum, $P^L(k)$, using a high precision CMB code (such as *CAMB* (Lewis, Challinor, & Lasenby 2000) or *CMBFAST* (Seljak & Zaldarriaga 1996)). The set of cosmological parameters assumed is the same as that of the simulated data if one is testing the accuracy of BAO scale extraction only. For real data, the set of cosmological parameters should be varied in a maximum likelihood analysis. Next, define a smooth reference spectrum for $P^L(k)$, $P^{\rm L}_{\rm ref}$, in the same manner as described in Step 1, using the same wavenumber bins. Finally, compute the ratio, $P^L/P^L_{\rm ref}$.

4. Modify the linear theory ratio, $P^L/P^L_{\rm ref}$, as follows:

$$R_{\rm L}(k) = \left[\frac{P^L(\alpha k)}{P^L_{\rm ref}(\alpha k)} - 1\right] \times W(k, k_{\rm nl}) + 1, \tag{49}$$

where the scale parameter α mimics a change in dark energy parameters (see Eq.[23]), and the Gaussian filter $W(k)$ describes the damping of the oscillations beyond some characteristic wavenumber:

$$W(k) = \exp\left(-\frac{k^2}{2k^2_{\rm nl}}\right), \tag{50}$$

with $k_{\rm nl}$ as a free parameter. Thus there are two free parameters, α and $k_{\rm nl}$.

5. Compute the likelihood for a grid of models, each specified by values of ($k_{\rm nl}$, α). The likelihood is given by (assuming Gaussian errors):

$$-2\ln L = \chi^2 = \sum_i \left(\frac{R^i - R^i_{\rm L}}{\sigma^i/P^i_{\rm ref}}\right)^2 \tag{51}$$

where the summation is over wavenumber and σ^i is the error on the power spectrum estimated in the $i^{\rm th}$ bin.

6. Derive confidence limits on α and $k_{\rm nl}$ in a likelihood analysis.

Figs.8-10 show the results from Angulo et al. (2008), from a high resolution simulation corresponding to a comoving volume of $2.41\,h^{-3}\,{\rm Gpc}^3$ (Angulo et al. 2008), and a ensemble of 50 low-resolution simulations (each with the same comoving volume but less resolution) to estimate the cosmic variance of the high resolution simulation. The dark matter haloes have mass in excess of $5.4 \times 10^{12}\,h^{-1}\,M_\odot$. The galaxies form an R-magnitude limited sample with a space density of $\bar{n} = 5 \times 10^{-4}\,h^3{\rm Mpc}^{-3}$.

Fig. 8 shows the values obtained for α from the power spectrum at various redshifts of the dark matter (triangles), dark matter haloes (circles) and galaxies (squares) (Angulo et al. 2008). There is a trend for the best-fitting value to deviate away from unity with decreasing redshift, although the result at $z = 0$ is still within 1σ of $\alpha = 1$ for dark matter and dark matter haloes. Fig.9 shows the best-fitting value of the damping scale $k_{\rm nl}$ as a function of redshift, for the same tracers of the matter density distribution as in Fig.8, in real-space (top) and redshift-space (bottom).

Fig.10 shows the recovered value of the scale parameter α for various galaxy samples (Angulo et al. 2008). Note that the accuracy and precision of the estimated α depends on the galaxy sample. For example, using a catalog of R-magnitude-limited galaxies with space density of $5\times10^{-4}\,h^3\,{\rm Mpc}^{-3}$ (Sample A) or red galaxies (Sample C), one could measure the BAO scale more accurately (smaller bias in α) and more precisely (smaller dispersion in α) than using a catalog of galaxies chosen by the strength of their emission lines (Sample D).

Note that the size of the systematic shift of the estimated α away from $\alpha = 1$ for the galaxy samples is comparable to the random measurement errors for the simulation (Angulo et al. 2008). It will require a larger simulation volume to reduce the size of random errors, and to ascertain whether such shifts reflect genuine limits of the method discussed here.

A more accurate model for the power spectrum is given by the "dewiggled" power spectrum (Tegmark et al. 2006; Eisenstein et al. 2006):

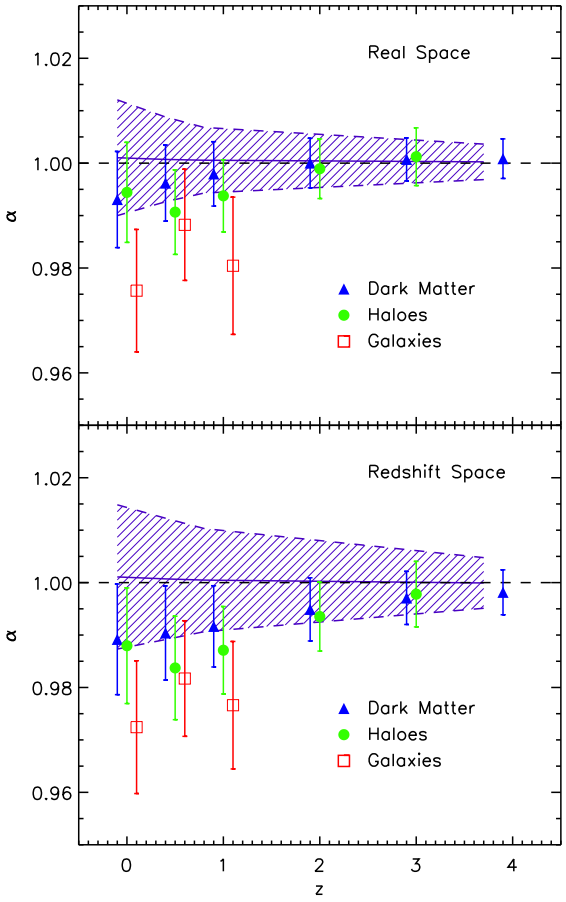

Figure 8. The best-fitting value of the scale factor α as a function of redshift, for different tracers of the matter density distribution, in real-space (top) and redshift-space (bottom) (Angulo et al. 2008)). The symbols show results from the high resolution simulation corresponding to a comoving volume of $2.41\,h^{-3}\,\mathrm{Gpc}^3$: dark matter (triangles), dark matter haloes with mass in excess of $5.4\times10^{12}\,h^{-1}\,M_\odot$ (circles) and galaxies from an R-magnitude limited sample with a space density of $\bar{n}=5\times10^{-4}\,h^3\,\mathrm{Mpc}^{-3}$ (squares). The error bars show the 1σ range on α, calculated from $\Delta\chi^2$. The hatched region shows the central 68% range of the results obtained using the dark matter in an ensemble of low resolution simulations. Recall that $\alpha=1$ corresponds to an unbiased measurement of the BAO scale (hence of dark energy parameters).

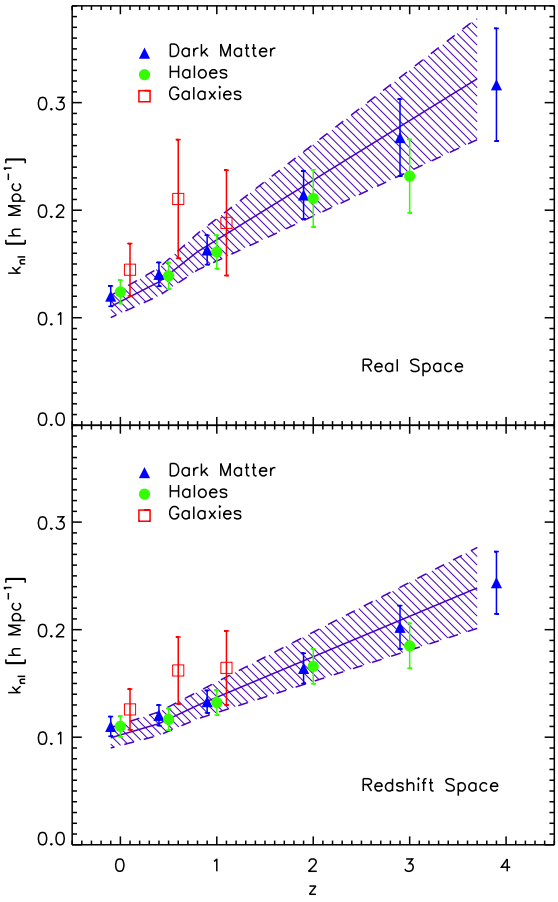

Figure 9. The best-fitting value of the damping scale $k_{\rm nl}$ as a function of redshift, for different tracers of the matter density distribution, in real-space (top) and redshift-space (bottom) (Angulo et al. 2008). The symbols show results from the high resolution corresponding to a comoving volume of $2.41\,h^{-3}\,\mathrm{Gpc}^3$: dark matter (triangles), dark matter haloes with mass in excess of $5.4\times10^{12}\,h^{-1}\,M_\odot$ (circles) and galaxies (squares). The error bars show the 1σ range on $k_{\rm nl}$. The hatched region shows the central 68% range of the results obtained using the dark matter in an ensemble of low resolution simulations.

$$P_{\rm dw}(k)=P_{\rm lin}(k)G(k)+P_{\rm nw}(k)\left[1-G(k)\right], \qquad (52)$$

where $P_{\rm lin}(k)$ is the linear theory power spectrum and $P_{\rm nw}(k)$ is a smooth, linear theory, cold dark matter only power spectrum, with the same shape as $P_{\rm lin}(k)$ but without any baryonic oscillations (i.e., $P^L_{\rm ref}$). The weight function $G(k)$ is given by

$$G(k)\equiv\exp\left[-(k/\sqrt{2}\,k_\star)^2\right], \qquad (53)$$

describing the transition from large scales ($k\ll k_\star$), where $P_{\rm dw}(k)$ follows linear theory, to small scales ($k\gg k_\star$) where the acoustic oscillations are completely damped by nonlinear effects.

Eq. (52) provides a phenomenological description of the modification of the BAO by nonlinear effects found in numerical simulations. Importantly, it can be justified using the renormalized perturbation theory (RPT) developed by Crocce & Scoccimarro (2006, 2008). According to RPT, the first term on the right hand side of Eq. (52) describes the growth of a single mode, quantified by the propagator function $G(k)$. In the high-k limit the propagator is given by the Gaussian form in Eq.(53) with $k_\star$ given by (Crocce & Scoccimarro 2006; Matsubara 2008)

$$k_\star=\left[\frac{1}{3\pi^2}\int{\rm d}k\,P_{\rm lin}(k)\right]^{-1/2}. \qquad (54)$$

The second term on the right hand side of Eq. (52) can be interpreted as the power generated by the coupling of Fourier modes on small scales, $P_{\rm mc}(k)$. The term $P_{\rm mc}(k)$ is negligible on large scales (small k), but dominates the total power on small scales (high k). For the scales relevant to the BAO analysis ($k\sim k_\star$), $P_{\rm mc}$ has a similar amplitude to $P_{\rm nw}(k)[1-G(k)]$.

The limitation of Eq. (52) can be explained by RPT as well (Crocce & Scoccimarro 2008)). According to RPT, the propagator $G(k)$ only behaves as a Gaussian in the high-k limit. In addition, the term $P_{\rm mc}$ shows acoustic oscillations, although of a much

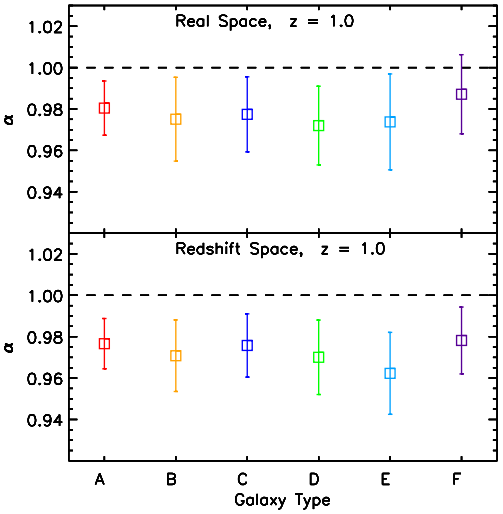

Figure 10. The recovered value of the scale parameter α for various galaxy samples (Angulo et al. 2008). Samples A is R-magnitude-limited to reach a space density of $5 \times 10^{-4}\, h^3\,\mathrm{Mpc}^{-3}$. Sample B is magnitude-limited to reach half the space density of sample A. Sample C contains the reddest 50% of galaxies from sample A, using the $R - I$ color. Sample D contains the 50% of galaxies from sample A with the strongest emission lines, using the equivalent width of OII[3727]. Sample E contains the bluest 50% of galaxies from sample A, using the $R - I$ color. Sample F contains the 50% of galaxies from sample A with the weakest emission lines, using the equivalent width of OII[3727]. The simulation corresponds to a comoving volume of $2.41\, h^{-3}\,\mathrm{Gpc}^3$. Recall that $\alpha = 1$ corresponds to an unbiased measurement of the BAO scale (hence of dark energy parameters).

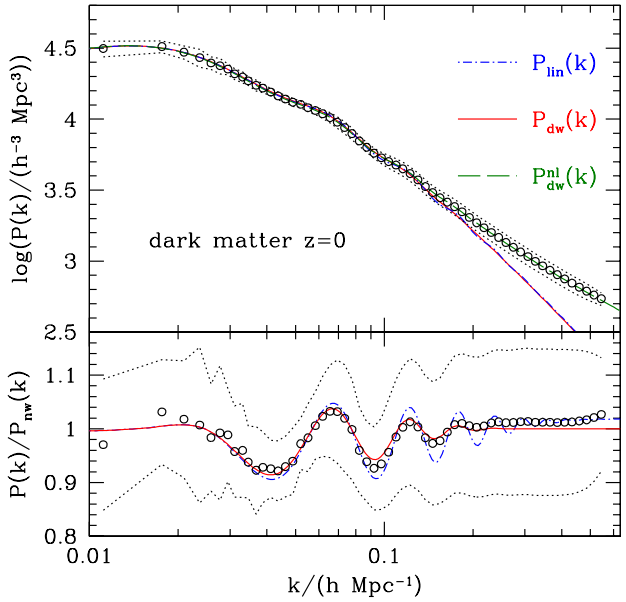

Figure 11. Results from the numerical simulations by Sanchez, Baugh, & Angulo (2008). Upper panel: A comparison of the real-space dark matter power spectrum averaged over the simulation ensemble (open points) with the linear theory power spectrum (dot-dashed line), the 'dewiggled' power spectrum from Eq. (52) (solid line), and its non-linear version from Eq. (55) (dashed line) computed with $Q = 13$ and $A = 1.5$. The dotted lines indicate the variance on $P(k)$ estimated from the ensemble. Lower panel: The ratio of these power spectra to $P_{\rm nw}(k)$.

smaller amplitude than $P(k)$, while $P_{\rm nw}(k)[1 - G(k)]$ is a smooth function.

Eq. (52) can be improved by modifying $P_{\rm nw}(k)$ to model the change in the overall shape of the power spectrum due to non-linear evolution:

$$P^{\rm nl}_{\rm dw}(k) = \left(\frac{1 + Q\,k^2}{1 + Ak + Bk^2}\right) P_{\rm dw}(k) = f(k) P_{\rm dw}(k). \qquad (55)$$

The factor $f(k)$ could also be used to model a scale dependent bias factor. This model for non-linear evolution is based on the Q-model of Cole et al. (2005), modified by the addition of a new parameter, B, in order to improve its accuracy at high k. Fixing $B = Q/10$ gives the approximate behavior of the non-linear power spectrum at large k (Sanchez, Baugh, & Angulo 2008).

Fig.11 shows a comparison of the real-space dark matter power spectrum averaged over the simulation ensemble (open points) with the linear theory power spectrum (dot-dashed line), the "dewiggled" power spectrum from Eq. (52) (solid line), and its non-linear version from Eq. (55) (dashed line) computed with $Q = 13$ and $A = 1.5$ (Sanchez, Baugh, & Angulo 2008). However, the improved modeling of the power spectrum still leads to biased estimate of α similar to that shown in Fig.8, but with $\alpha > 1$ (Sanchez, Baugh, & Angulo 2008).

The biased estimates of α from the measured power spectra (see Figs.8 and 10) are a consequence of the mode-coupling shifts due to nonlinear effects (Crocce & Scoccimarro 2008). This may indicate a limit to the accuracy with which the BAO scale can be extracted from power spectrum data. In Fourier space, systematic effects such as redshift-space distortions and scale-dependent bias are important, and have to be minimized by dividing the measured power spectrum by a smooth reference power spectrum. This division by the smooth reference power spectrum leads to information loss that degrades the BAO scale accuracy and precision (Sanchez, Baugh, & Angulo 2008). However, larger volume simulations will be needed to quantify the limit of accuracy of the $P(k)$ method of BAO analysis.

4.2 Using two-point correlation functions to probe BAO

To extract the BAO scales, we can also compute the two-point correlation function of galaxies in comoving coordinates. For spherically-averaged data, the BAO scale corresponds to a peak around the scale of the sound horizon at the drag epoch. Eisenstein et al. (2005) first demonstratedthis with real data. Hutsi (2006) found similar results.

Definition of the two-point correlation function $\xi(\mathbf{r})$

The two-point correlation function ξ is defined as

$$\xi(\mathbf{r}) \equiv \langle \delta(\mathbf{x} + \mathbf{r}) \delta(\mathbf{x}) \rangle. \qquad (56)$$

Thus the power spectrum and $\xi(\mathbf{r})$ are related by

$$P(\mathbf{k}) \equiv \left|\delta_{\mathbf{k}}\right|^2 = \int \xi(\mathbf{r})\, e^{i\mathbf{k}\cdot\mathbf{r}}\, d^3\mathbf{r}, \qquad (57)$$

where $\delta_{\mathbf{k}}$ is the Fourier transform of the matter density perturbation $\delta(\mathbf{r})$ (see Eq.[27]).

Measurement of the two-point correlation function $\xi(\mathbf{r})$

The two-point galaxy correlation function, ξ, can be measured

by comparing the actual galaxy distribution to a catalog of randomly distributed galaxies. These randomly distributed galaxies have the same redshift, magnitude, and mask constraints as the real data. The pairs of galaxies are counted in bins of separation along the line of sight, π_s, and transverse to the line of sight, r_p, to estimate $\xi(r_p,\pi_s)$. In converting from redshift to distance, a fiducial model must be assumed, usually a flat universe model dominated by a cosmological constant, with $\Omega_m=0.3$, $\Omega_\Lambda=0.7$. Hence it is important to iterate the final results by changing the fiducial model to the bestfit model derived from the data.

Each galaxy and random galaxy can be given a weighting factor to account for both selection effects and to optimize the statistics. For example, to minimize the variance on the estimated $\xi(\mathbf{s})$ when the survey selection function $n(z_i)$ varies significantly, one can introduce the so-called "minimum-variance weighting" (Davis & Huchra 1982; Davis & Peebles 1983):

$$w_i=\frac{1}{1+4\pi n(z_i)J_3(s)}, \tag{58}$$

where the separation $s\equiv\sqrt{\pi_s^2+r_p^2}$, $n(z)$ is the galaxy density distribution, and

$$J_3(s)=\int_0^s \xi(s')\,s'^2{\rm d}s'. \tag{59}$$

Hawkins et al. (2003) used $n(z)$ from the random catalog to ensure that the weights vary smoothly with redshift, and they found that results are insensitive to the precise form of J_3. Each galaxy pair (i, j) is given a weight $w_fw_iw_j$ (with w_f correcting for galaxies not observed due to effects such as fibre collisions), while each galaxy-random and random-random pair is given a weight w_iw_j.

An often-used minimum-variance estimator of ξ is that of Landy & Szalay (1993):

$$\xi(r_p,\pi_s)=\frac{DD-2DR+RR}{RR}, \tag{60}$$

where r_p and π_s denote the transverse and line-of-sight separations in redshift space respectively. DD is the normalized sum of weights of galaxy-galaxy pairs with separation (r_p, π_s), RR is the normalized sum of weights of random-random pairs with the same separation in the random catalog and DR is the normalized sum of weights of galaxy-random pairs with the same separation. DR is calculated by overlaying the real galaxy catalog and the simulated random galaxy catalog. DD, RR, and DR are normalized through dividing by the total number of pairs in each. Spherically averaging $\xi(r_p,\pi_s)$ at constant $s=\sqrt{{\pi_s}^2+{r_p}^2}$ gives the redshift-space correlation function $\xi(s)$. Both Eisenstein et al. (2005) and Okumura et al. (2008) used the Landy & Szalay estimator in Eq.(60) to analyze SDSS LRG data.

If the rms scatter on $P(k)$, $\sigma_P^2(k)$, is computed (see Sec.4.1), the covariance of the two-point correlation function can be calculated using (Cohn 2006; Smith, Scoccimarro, & Sheth 2008):

$$\begin{aligned} C_\xi(r,r') &\equiv \left\langle\left[\xi(r)-\bar\xi(r)\right]\left[\xi(r')-\bar\xi(r')\right]\right\rangle \\ &= \int\frac{{\rm d}k\,k^2}{2\pi^2}\,j_0(kr)j_0(kr')\sigma_P^2(k), \end{aligned} \tag{61}$$

where $\xi(r)$ and $\bar\xi(r)$ are the correlation function and its mean respectively.

The BAO scale shown in Fig.1 is measured from the spherically-averaged redshift-space correlation function from SDSS LRG sample by Eisenstein et al. (2005). There is no verifiable detection of the radial and transverse BAO scales from current data (Okumura et al. 2008; Gaztanaga, Cabre, & Hui 2008). This may be an indication of systematic uncertainties.

Mitigation of systematic effects in BAO scale extraction from $\xi(\mathbf{r})$

Simulated data must be used to study how the BAO scale extraction from the measured galaxy two-point correlation function is affected by systematic effects. Using 50 low resolution N-body simulations (each with a comoving volume of $2.41\,h^{-3}\,{\rm Gpc}^3$ and with the dark matter followed using 448^3 particles), Sanchez, Baugh, & Angulo (2008) found that the BAO signature in the two-point correlation function is less affected by scale dependent effects than that in the power spectrum.

The two-point correlation function can be obtained by taking the Fourier transform of Eq. (52):

$$\xi_{\rm dw}(r)=\xi_{\rm lin}(r)\otimes\tilde G(r)+\xi_{\rm nw}(r)\otimes(1-\tilde G(r)), \tag{62}$$

where the symbol $\otimes$ denotes a convolution, and $\tilde G(r)$ is the Fourier transform of $G(k)$. The first term contains the information about the acoustic oscillations; it represents the convolution of the linear theory correlation function with a Gaussian kernel. This convolution implies that in the correlation function, the damping of the higher harmonic oscillations causes the acoustic peak to broaden and shift to smaller scales (Smith, Scoccimarro, & Sheth 2008; Crocce & Scoccimarro 2008).

Fig. 12 compares the mean $z=0$ real-space correlation function of the dark matter measured from an ensemble of simulations (open points) with the following models for the correlation function: (i) the linear theory correlation function $\xi_{\rm lin}(r)$ (solid line), (ii) a nonlinear correlation function $\xi^{\rm nl}(r)$ computed using `halofit`, without any damping of the acoustic oscillations (short-dashed line), (iii) the dewiggled linear theory correlation function $\xi_{\rm dw}(r)$, computed as described by Eq. (62) (long-dashed line) and (iv) a dewiggled correlation function nonlinearized using `halofit` $\xi^{\rm nl}_{\rm dw}(r)$ (dot-dashed line) (Sanchez, Baugh, & Angulo 2008). The error bars indicate the variance between the correlation functions measured from the different realizations in the simulation ensemble.

Fig. 12 shows that the acoustic peak in the two-point correlation function at redshift $z=0$ shows strong deviations from the predictions of linear theory. Clearly, the linear theory dewiggled correlation function from Eq. (62) gives a very good description of the results of numerical simulations; this indicates that the damping of the oscillations is the most important effect to include in the modeling of the real space correlation function on large scales. The incorporation of the full change in the shape of $P(k)$ due to nonlinear evolution produces very little difference in the shape of the acoustic peak in the correlation function, but this effect might be important on intermediate scales ($r\simeq 70\,h^{-1}\,{\rm Mpc}$).

The scale parameter from Eq.(23) corresponds to an equivalent shift from scale $r_{\rm true}$ to $r_{\rm app}=r_{\rm true}/\alpha$ in the two-point correlation function. Deviation from $\alpha=1$ indicates biased estimate of the BAO scale, and the uncertainty on α indicates the precision of the BAO scale measurement. Sanchez, Baugh, & Angulo (2008) used Eq. (62) to analyze an ensemble of 50 low resolution N-body simulations (each with a comoving volume of $2.41\,h^{-3}\,{\rm Gpc}^3$) (Sanchez, Baugh, & Angulo 2008). The estimated scale parameter is slightly biased: $\alpha=0.996\pm0.006$ at $z=0$, $\alpha=0.998\pm0.004$ at $z=0.5$ and $\alpha=0.997\pm0.003$ at $z=1$. The constraints on α become tighter with increasing redshift. This is because the higher harmonic oscillations are less damped as redshift increases (which accompanies an increase in the range of wavenumbers over which density perturbations are linear), thus the position of the BAO peak

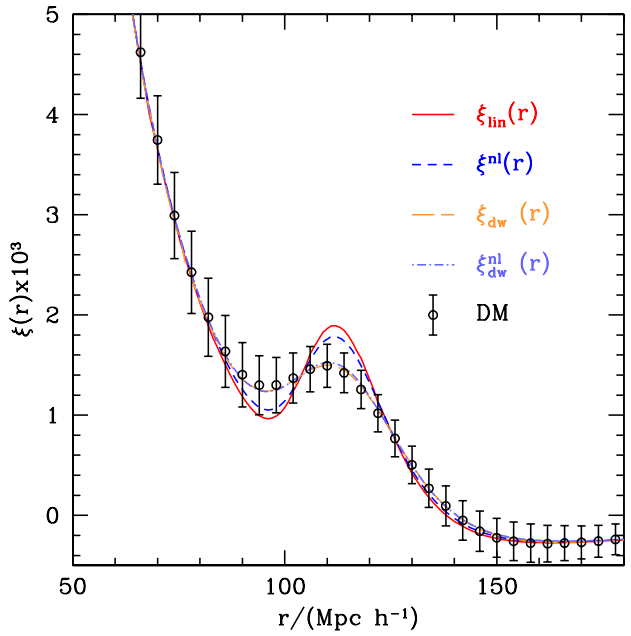

Figure 12. Comparison by Sanchez, Baugh, & Angulo (2008) of the $z = 0$ real-space dark matter two-point correlation function averaged over the ensemble of simulations (open points) with: (i) the linear theory correlation function $\xi_{\rm lin}(r)$ (solid line), (ii) an estimate of the nonlinear correlation function $\xi^{\rm nl}(r)$ computed using `halofit` without damping of the acoustic oscillations (dashed line), (iii) the dewiggled linear theory correlation function $\xi_{\rm dw}(r)$ defined by Eq. (62) (dot-dashed line) and (iv) a dewiggled correlation function after being nonlinearized using `halofit` $\xi^{\rm nl}_{\rm dw}(r)$ (long-dashed line). The error bars indicate the rms scatter between the different realizations in the ensemble of simulations.

can be more precisely determined. The deviation from $\alpha = 1$ indicates the limitation of Eq. (62) in describing the full shape of the correlation function.

The model of Eq. (62) can be improved by utilizing the BAO information contained in $\xi_{\rm mc}(r)$, the correlation function generated by the coupling of Fourier modes on small scales. According to renormalized perturbation theory (RPT), the main contribution to $\xi_{\rm mc}(r)$ on the scale of BAO is of the form (Crocce & Scoccimarro 2008)

$$\xi_{\rm mc}(r) \propto \xi'_{\rm lin}\, \xi^{(1)}_{\rm lin}(r), \tag{63}$$

where $\xi'_{\rm lin}$ is the derivative of the linear theory correlation function and

$$\xi^{(1)}_{\rm lin}(r) \equiv \hat{r}\cdot\nabla^{-1}\xi_{\rm lin}(r) = 4\pi \int P_{\rm lin}(k)\, j_1(kr) k\, {\rm d}k. \tag{64}$$

Thus an improved model of the correlation function is given by (Crocce & Scoccimarro 2008)

$$\xi_{\rm nl}(r) = \xi_{\rm lin}(r) \otimes \tilde{G}(r) + A_{\rm mc}\, \xi'_{\rm lin}\xi^{(1)}_{\rm lin}(r), \tag{65}$$

where $A_{\rm mc}$ is a free parameter. The second term in Eq.(65) can describe the shape of the residuals of the measured correlation function with respect to $\xi_{\rm lin} \otimes \tilde{G}$ close to the BAO peak. At smaller scales, where the approximation is not so accurate, the model underestimates the correlation function (Sanchez, Baugh, & Angulo 2008). Applying Eq.(65) to an ensemble of 50 low resolution N-body simulations (each with a comoving volume of $2.41\, h^{-3}\,{\rm Gpc}^3$), Sanchez, Baugh, & Angulo (2008) found that the scale parameter is measured more accurately: $\alpha = 1.003 \pm 0.008$ at $z = 0$, $\alpha = 1.002 \pm 0.005$ at $z = 0.5$ and $\alpha = 1.000 \pm 0.003$ at $z = 1$. This indicates that the implementation of a full calculation of $\xi_{\rm mc}$ using RPT over the full range of scales included in the analysis can lead to unbiased estimate of the BAO scale. Note also that reducing the bias in the estimate of the BAO scale generally leads to an increase in its statistical scatter.

In current analysis techniques explored, the correlation function analysis leads to more accurate and precise estimate of the BAO scale than the power spectrum method (Sanchez, Baugh, & Angulo 2008). The main reason for this is that the correlation function is less affected by scale-dependent effects than the power spectrum. Thus in a correlation function analysis, the entire correlation function can be modeled (including the large scale shape), while in the power spectrum analysis, the information on amplitude and large scale shape is discarded in order to remove sensitivity to systematic effects such as nonlinear effects and redshift-space distortions (Sanchez, Baugh, & Angulo 2008).

5 FUTURE PROSPECTS FOR BAO MEASUREMENTS

Given real or simulated galaxy redshift survey data, one would need to extract the radial and transverse BAO scales from the data in order to estimate $H(z)$ and $D_A(z)$, *before* measuring the dark energy parameters, as illustrated by Secs.4.1 and 4.2. Robust forecast can only come from a Monte Carlo based approach that begins with extracting the radial and transverse BAO scales from realistically simulated galaxy catalogs.

Most of the BAO forecasts have been done using the Fisher matrix formalism, which gives the smallest possible statistical uncertainties. The Fisher information matrix of a given set of parameters, $\mathbf{s}$, approximately quantifies the amount of information on $\mathbf{s}$ that we "expect" to get from our future data. The Fisher matrix can be written as

$$F_{ij} = -\frac{\partial^2 \ln L}{\partial s_i \partial s_j}, \tag{66}$$

where L is the likelihood function, the expected probability distribution of the observables given parameters $\mathbf{s}$.

The Cramér-Rao inequality (Kendall & Stuart 1969) states that no unbiased method can measure the i-th parameter with standard deviation less than $1/\sqrt{F_{ii}}$ if other parameters are known, and less than $\sqrt{(\mathbf{F}^{-1})_{ii}}$ if other parameters are estimated from the data as well. Note that the derivatives in Equation (66) are calculated assuming that the cosmological parameters are given by an a priori model, and thus the errors on the parameters are somewhat dependent on the assumed model. It is straightforward to apply Eq.(66). For Gaussian distributed measurements, $L \propto \exp(-\chi^2/2)$.

The Fisher matrix method allows an estimate of expected measurement uncertainties on $H(z)$ and $D_A(z)$ from a future galaxy redshift survey based on the assumed survey parameters, *without* analyzing simulated galaxy catalogs to extract the BAO scales. While the Fisher matrix forecasts are likely too optimistic, they are easy and straightforward to make, thus provide the most convenient way to estimate the expected constraints on dark energy from future galaxy redshift surveys. Here we discuss the Fisher matrix forecast methodology in detail.

In the limit where the length scale corresponding to the survey volume is much larger than the scale of any features in $P_g(k)$, we can assume that the likelihood function for the band powers of a galaxy redshift survey is Gaussian, and given by

Eq.(46) with a measurement error in $\ln P(\mathbf{k})$ that is proportional to $[V_{eff}(\mathbf{k})]^{-1/2}$, with the effective volume of the survey defined as (see Eq.[47]):

$$V_{eff}(k,\mu) \equiv \int d\mathbf{r}^3 \left[\frac{n(\mathbf{r})P_g(k,\mu)}{n(\mathbf{r})P_g(k,\mu)+1}\right]^2 = \left[\frac{nP_g(k,\mu)}{nP_g(k,\mu)+1}\right]^2 V_{survey}, \quad (67)$$

where the comoving number density n is assumed to only depend on the redshift (and constant in each redshift slice) for simplicity in the last part of the equation.

In order to propagate the measurement error in $\ln P_g(\mathbf{k})$ into measurement errors for the parameters p_i, we can use Eq.(66), and that

$$\mathcal{L}\left[P(\mathbf{k})\right] = \mathcal{L}(p_i), \quad (68)$$

with $\mathcal{L}\left[P(\mathbf{k})\right]$ given by Eq.(46). Ignoring the subdominant normalization factors, this gives an approximated Fisher matrix (Tegmark 1997)

$$F_{ij} = \int_{k_{min}}^{k_{max}} \frac{\partial \ln P_g(\mathbf{k})}{\partial p_i}\frac{\partial \ln P_g(\mathbf{k})}{\partial p_j} V_{eff}(\mathbf{k}) \frac{d\mathbf{k}^3}{2\,(2\pi)^3} \quad (69)$$

where p_i are the parameters to be estimated from data, and the derivatives are evaluated at parameter values of the fiducial model. Note that the Fisher matrix F_{ij} is the inverse of the covariance matrix of the parameters p_i if the p_i are Gaussian distributed.

"Wiggles Only" Method

In order to arrive at robust BAO forecasts, we may use the information contained in the BAO peaks only, and discard the information contained in the broad shape of $P_g(k)$ (Blake & Glazebrook 2003; Seo & Eisenstein 2007). The measurement of the BAO peaks gives measurements of $s/D_A(z)$ and $s\,H(z)$ (see Eq.[1]).

Note that Eq.(69) can be rewritten as

$$F_{ij} = V_{survey}\int_{-1}^{1} d\mu \int_{k_{min}}^{k_{max}} \frac{\partial P_g(k,\mu)}{\partial p_i}\frac{\partial P_g(k,\mu)}{\partial p_j} \cdot \left[\frac{1}{P_g(k,\mu)+n^{-1}}\right]^2 \frac{2\pi k^2 dk}{2\,(2\pi)^3}, \quad (70)$$

where $\mu = \hat{\mathbf{k}}\cdot\hat{\mathbf{r}}$, with $\hat{\mathbf{r}}$ denoting the unit vector along the line of sight.

Seo & Eisenstein (2007) obtained simple fitting formulae for estimated errors in $s/D_A(z)$ and $s\,H(z)$ by approximating Eq.(70) with

$$F_{ij} \simeq V_{survey}\int_{-1}^{1} d\mu \int_{k_{min}}^{k_{max}} \frac{\partial P_b(k,\mu|z)}{\partial p_i}\frac{\partial P_b(k,\mu|z)}{\partial p_j} \cdot \left[\frac{1}{P_g^{lin}(k,\mu|z)+n^{-1}}\right]^2 \frac{2\pi k^2 dk}{2\,(2\pi)^3}, \quad (71)$$

where $P_b(k,\mu|z)$ is the power spectrum that contains baryonic features. The linear galaxy power spectrum

$$P_g^{lin}(k,\mu|z) = P_{g,r}^{lin}(k|z)\,R(\mu) \quad (72)$$

$$P_{g,r}^{lin}(k|z) = [b(z)]^2\left[\frac{G(z)}{G(0)}\right]^2 P_m^{lin}(k|z=0) \quad (73)$$

where $P_{g,r}^{lin}(k|z)$ is the linear galaxy power spectrum in real space, $b(z)$ is the bias factor, $G(z)$ is the growth factor, and $P_m^{lin}(k|z=0)$ is the present day linear matter power spectrum. $R(\mu)$ is the linear redshift distortion factor given by (see Eq.[18]) (Kaiser 1987)

$$R(\mu) = \left(1+\beta\mu^2\right)^2. \quad (74)$$

The power spectrum that contains baryonic features, $P_b(k,\mu)$, is given by (Seo & Eisenstein 2007)

$$P_b(k,\mu|z) = \sqrt{8\pi^2}A_0\,P_g^{lin}(k_{0.2},\mu|z)\frac{\sin(x)}{x}\cdot \cdot\exp\left[-(k\Sigma_s)^{1.4}-\frac{k^2\Sigma_{nl}^2}{2}\right], \quad (75)$$

where we have define

$$k_{0.2} \equiv 0.2\,h\,\mathrm{Mpc}^{-1} \quad (76)$$

$$x \equiv \left(k_\perp^2 s_\perp^2 + k_\parallel^2 s_\parallel^2\right)^{1/2} \quad (77)$$

$$k_\parallel = \mathbf{k}\cdot\hat{\mathbf{r}} = k\mu \quad (78)$$

$$k_\perp = \sqrt{k^2-k_\parallel^2} = k\sqrt{1-\mu^2}. \quad (79)$$

The nonlinear damping scale

$$\Sigma_{nl}^2 = (1-\mu^2)\Sigma_\perp^2 + \mu^2\Sigma_\parallel^2$$

$$\Sigma_\parallel = \Sigma_\perp(1+f_g)$$

$$\Sigma_\perp = 12.4\,h^{-1}\mathrm{Mpc}\left(\frac{\sigma_8}{0.9}\right)\cdot 0.758\,\frac{G(z)}{G(0)}\,p_{NL} = 8.355\,h^{-1}\mathrm{Mpc}\left(\frac{\sigma_8}{0.8}\right)\cdot\frac{G(z)}{G(0)}\,p_{NL}, \quad (80)$$

where the growth rate $f_g = d\ln G(z)/d\ln a$. The parameter p_{NL} indicates the remaining level of nonlinearity in the data; with $p_{NL}=0.5$ (50% nonlinearity) as the best case, and $p_{NL}=1$ (100% nonlinearity) as the worst case (Seo & Eisenstein 2007). For a fiducial model based on WMAP3 results (Spergel et al. 2007) ($\Omega_m=0.24$, $h=0.73$, $\Omega_\Lambda=0.76$, $\Omega_k=0$, $\Omega_b h^2=0.0223$, $\tau=0.09$, $n_s=0.95$, $T/S=0$), $A_0=0.5817$, $P_{0.2}=2710\,\sigma_{8,g}^2$, and the Silk damping scale $\Sigma_s=8.38\,h^{-1}$Mpc (Seo & Eisenstein 2007).

Defining

$$p_1 = \ln s_\perp^{-1} = \ln(D_A/s), \quad (81)$$

$$p_2 = \ln s_\parallel = \ln(sH), \quad (82)$$

substituting Eq.(75) into Eq.(71), and making the approximation of $\cos^2 x \sim 1/2$, we find

$$F_{ij} \simeq V_{survey}A_0^2\int_0^1 \mathrm{d}\mu\, f_i(\mu)\,f_j(\mu)\int_0^{k_{max}}\mathrm{d}k\,k^2\cdot \cdot\left[\frac{P_m^{lin}(k|z=0)}{P_m^{lin}(k_{0.2}|z=0)}+\frac{1}{nP_g^{lin}(k_{0.2},\mu|z)\,e^{-k^2\mu^2\sigma_r^2}}\right]^{-2} \cdot\exp\left[-2(k\Sigma_s)^{1.4}-k^2\Sigma_{nl}^2\right], \quad (83)$$

where $P_g^{lin}(k_{0.2},\mu|z)$ is given by Eq.(72) with $k=k_{0.2}$, and $k_{max}=0.5\,h\mathrm{Mpc}^{-1}$ (Seo & Eisenstein 2007). Note that we have added the damping factor, $e^{-k^2\mu^2\sigma_r^2}$, due to redshift uncertainties, with

$$\sigma_r = \frac{\partial r}{\partial z}\,\sigma_z \quad (84)$$

where r is the comoving distance from Eq.(2). The functions $f_i(\mu)$ are given by

$$f_1(\mu) = \partial\ln x/\partial p_1 = \mu^2-1 \quad (85)$$

$$f_2(\mu) = \partial\ln x/\partial p_2 = \mu^2. \quad (86)$$

The square roots of diagonal elements of the inverse of the Fisher matrix of Eq.(83) give the estimated smallest possible measurement errors on $s_\perp^{-1}$ and $s_\parallel$. The estimated errors are *independent* of cosmological priors, thus scale with (area)$^{-1/2}$, for a fixed survey depth.

Full $P(k)$ Method

Since the full $P_g(k)$ is measured from a galaxy redshift survey, it is also useful to make forecasts of dark energy constraints using the full $P_g(k)$. The observed galaxy power spectrum can be reconstructed using a particular reference cosmology, including the effects of bias and redshift-space distortions (Seo & Eisenstein 2003):

$$\begin{aligned} & P_g^{obs}(k_\perp^{ref}, k_\parallel^{ref}) \\ = \; & \frac{\left[D_A(z)^{ref}\right]^2 H(z)}{\left[D_A(z)\right]^2 H(z)^{ref}} b^2 \left(1+\beta\,\mu^2\right)^2 \left[\frac{G(z)}{G(0)}\right]^2 P_m(k)_{z=0} \\ & + P_{shot}, \end{aligned} \tag{87}$$

where $\mu = \mathbf{k}\cdot\hat{\mathbf{r}}/k$, with $\hat{\mathbf{r}}$ denoting the unit vector along the line of sight; $\mathbf{k}$ is the wavevector with $|\mathbf{k}| = k$. Hence $\mu^2 = k_\parallel^2/k^2 = k_\parallel^2/(k_\perp^2 + k_\parallel^2)$. The values in the reference cosmology are denoted by the subscript "ref", while those in the true cosmology have no subscript. Note that

$$k_\perp^{ref} = k_\perp D_A(z)/D_A(z)^{ref}, \qquad k_\parallel^{ref} = k_\parallel H(z)^{ref}/H(z). \tag{88}$$

Eq.(87) characterizes the dependence of the observed galaxy power spectrum on $H(z)$ and $D_A(z)$ due to BAO, as well as the sensitivity of a galaxy redshift survey to the linear redshift-space distortion parameter β (see Eq.[19]).

The observed galaxy power spectrum in a given redshift shell centered at redshift z_i can be described by a set of parameters, $\{H(z_i),\ D_A(z_i),\ \overline{G(z_i)},\ \beta(z_i),\ P_{shot}^i,\ n_S,\ \omega_m,\ \omega_b\}$, where n_S is the power-law index of the primordial matter power spectrum, $\omega_m = \Omega_m h^2$, and $\omega_b = \Omega_b h^2$ (h is the dimensionless Hubble constant). Note that $P(k)$ does *not* depend on h if k is in units of Mpc^{-1}, since the matter transfer function $T(k)$ only depends on ω_m and ω_b (Eisenstein & Hu 1998),[1] if the dark energy dependence of $T(k)$ can be neglected. Note also that $T(k)$ is normalized such that $T(k\to 0) = 1$. Since $G(z)$, b, and the power spectrum normalization P_0 are completely degenerate in Eq.(87), they can be combined into a single parameter, $\overline{G(z_i)} \equiv b(z)\,G(z)\,P_0^{1/2}/G(0)$.

The square roots of diagonal elements of the inverse of the full Fisher matrix of Eq.(69) gives the estimated smallest possible measurement errors on the assumed parameters. The parameters of interest are $\{H(z_i),\ D_A(z_i),\ \beta(z_i)\}$, all other parameters are marginalized over. Note that the estimated errors we obtain are *independent* of cosmological priors since no priors are explicitly imposed, thus scale with (area)$^{-1/2}$ for a fixed survey depth. Priors on $\omega_m, \omega_b, \Omega_k$, and n_S will be required to obtain the errors on dark energy parameters if only BAO data are considered.

In order to compare the "wiggles only" method and the full $P(k)$ method for BAO forecast, we must include the nonlinear effects in the same way in both methods. We can include nonlinear effects in the full power spectrum calculation by modifying the derivatives of $P_g(\mathbf{k})$ with respect to the parameters p_i as follows (Seo & Eisenstein 2007)

$$\frac{\partial P_g(k,\mu|z)}{\partial p_i} = \frac{\partial P_g^{lin}(k,\mu|z)}{\partial p_i}\cdot\exp\left(-\frac{1}{2}\,k^2\Sigma_{nl}^2\right). \tag{89}$$

The damping is applied to derivatives of $P_g(k)$, rather than $P_g(k)$, to ensure that no information is extracted from the damping itself (Seo & Eisenstein 2007). Eq.(70) becomes

$$\begin{aligned} F_{ij} \;=\; & V_{survey}\int_{-1}^{1} d\mu \int_{k_{min}}^{k_{max}} \frac{\partial \ln P_g^{lin}(k,\mu)}{\partial p_i}\frac{\partial \ln P_g^{lin}(k,\mu)}{\partial p_j}\cdot \\ & \cdot\left[\frac{nP_g^{lin}(k,\mu)}{nP_g^{lin}(k,\mu)+1}\right]^2 e^{-k^2\Sigma_{nl}^2}\,\frac{2\pi k^2 dk}{2\,(2\pi)^3}. \end{aligned} \tag{90}$$

Under the same assumptions, the full $P_g(k)$ method can boost the Figure-of-Merit (FoM) for constraining dark energy by a factor of ∼3-4, compared to the "wiggles only" method (see e.g., Wang (2009)), if no other data or priors are added, and redshift-space distortions are marginalized over in the $P(k)$ method (Seo & Eisenstein 2003; Wang 2006). The two methods give very similar constraints on the BAO scales $s/D_A(z)$ and $s\,H(z)$ (Seo & Eisenstein 2007; Wang 2009); the difference comes in the use of additional information from the broad shape of $P_g(k)$ in the full $P(k)$ method.

Galaxy Number Density

For a given galaxy redshift survey, the galaxy number density $n(z)$ and bias function $b(z)$ should be modeled using available data and supplemented by cosmological N-body simulations that include galaxies (Angulo et al. 2008). Since $n(z)$ and $b(z)$ depend on survey parameters such as the flux limit and the target selection method and efficiency, a more generic galaxy number density given by assuming $nP_g^r(k_{0.2}|z) = 3$ is often used in Fisher matrix forecasts (Seo & Eisenstein 2007), where $P_g^r(k_{0.2}|z)$ is the real space power spectrum of galaxies at $k = 0.2\,h\,\mathrm{Mpc}^{-1}$ and redshift z. Note that this assumption means

$$nP_g^r(k_{0.2}|z) = P_m(k_{0.2}|0)\,n(z)\,b^2(z)\left[\frac{G(z)}{G(0)}\right]^2 = 3, \tag{91}$$

where $G(z)$ is the growth factor, and $b(z)$ is the bias factor. Assuming a fiducial cosmological model that fits all current observational data, $G(z)$ decreases by about a factor of 2 from $z=0$ to $z=2$, while $b(z)$ may increase with z somewhat and is dependent on the type of galaxies sampled by the survey.

For an ambitious yet feasible galaxy redshift survey of Hα emission line galaxies, using a fully empirical $n(z)$ derived from current observational data (Geach et al. 2009), and a bias factor $b(z)$ derived from cosmological N-body simulations calibrated with current observational data (Orsi et al. 2010), $nP_g^r(k_{0.2}|z) > 3$ near the median redshift ($z_m \sim 1$), while $nP_g^r(k_{0.2}|z) < 3$ at $z \sim 2$, assuming a realistic efficiency for galaxy spectroscopy (Cimatti et al. 2009). This is as expected. The observed galaxy number density $n(z)$ from a flux-limited survey peaks at the median redshift, and decreases sharply in the high z tail, as the number of galaxies fainter than the flux limit increases. The increase in the bias factor $b(z)$ is not fast enough to compensate for the decrease in both $G(z)$ and $n(z)$ to satisfy $nP_g^r(k_{0.2}|z) \geqslant 3$ at $z\sim 2$. Therefore, assuming $nP_g^r(k_{0.2}|z) = 3$ is likely too optimistic, while assuming $n(z)\,[b(z)/b(0)]^2\,P_g^r(k_{0.2}|z=0) = 3$ could be a conservative alternative in Fisher matrix forecasts for a generic galaxy redshift survey (Wang 2009).

[1] Massive neutrinos can suppress the galaxy power spectrum amplitudes by $\gtrsim 4\%$ on BAO scales (Hu, Eisenstein, & Tegmark 1998; Eisenstein & Hu 1999).

6 PROBING THE COSMIC GROWTH RATE USING REDSHIFT SPACE DISTORTIONS

A galaxy redshift survey can allow us to measure both $H(z)$ and $f_g(z)$ (Guzzo et al. 2007; Wang 2008). The measurement of $f_g(z)$ can be obtained through independent measurements of redshift-space distortion parameter $\beta = f_g(z)/b$ (Kaiser 1987) and the bias parameter $b(z)$ (which describes how light traces mass) (Guzzo et al. 2007).

6.1 Measuring redshift-space distortion parameter β

The parameter β can be measured directly from galaxy redshift survey data by studying the observed two-point redshift-space correlation function (Hawkins et al. 2003; Tegmark et al. 2006; Ross et al. 2007; daAngela et al. 2006). Hamilton (1998) reviewed various techniques for measuring β.

Peculiar velocities of galaxies lead to systematic differences between redshift-space and real-space measurements, and the effects are a combination of large-scale coherent flows induced by the gravity of large-scale structure, and a small-scale random velocity of each galaxy (see Sec.3.2). The large-scale flows compress the contours of $\xi(r_p, \pi_s)$ along the π_s direction (along the line of sight), with the degree of compression determined by β. Kaiser (1987) showed that the coherent infall velocities lead to the following relation between the redshift-space power spectrum $P_s(k)$ and the real-space power spectrum $P_r(k)$ (Kaiser 1987), see Eq.[18]):

$$P_s(k,\mu) = \left(1+\beta\mu^2\right)^2 P_r(k,\mu), \tag{92}$$

where $\mu = \mathbf{k}\cdot\hat{\mathbf{r}}/k$, with $\hat{\mathbf{r}}$ denoting the unit vector along the line of sight; $\mathbf{k}$ is the wavevector with $|\mathbf{k}| = k$. The small-scale random motion of galaxies leads to a smearing in the radial direction (the "Finger of God" effect).

Linear Regime

In the linear regime, the ratio of the spherically-averaged two point correlation function in redshift-space and real space is given by

$$\frac{\xi(s)}{\xi(r)} = 1 + \frac{2\beta}{3} + \frac{\beta^2}{5}. \tag{93}$$

Recall that the redshift-space correlation function $\xi(s)$ can be obtained by spherically averaging the measured redshift-space correlation function $\xi(r_p, \pi_s)$ (see Eq.[60]) at constant $s = \sqrt{\pi_s^2 + r_p^2}$ (see Sec.4.2).

Since the two-point correlation function is defined by the joint probability of finding galaxies centered within the volume elements dV_1 and dV_2 at a given separation, the projected correlation function (integrated along the line-of-sight) should be the same in real and redshift space – both give the two-point angular correlation function. Thus the real-space correlation function $\xi(r)$ can be estimated by inverting the projected redshift-space correlation function $\Xi(r_p)$ (i.e., the angular correlation function) (Davis & Peebles 1983):

$$\xi(r) = -\frac{1}{\pi}\int_r^\infty \mathrm{d}r_p\, \frac{\Xi'(r_p)}{(r_p^2 - r^2)^{1/2}} \tag{94}$$

where

$$\Xi(r_p) = 2\int_0^\infty \mathrm{d}\pi_s\, \xi(r_p, \pi_s). \tag{95}$$

Fig.13 shows the ratio of $\xi(s)$ to $\xi(r)$ for the 2dFGRS data

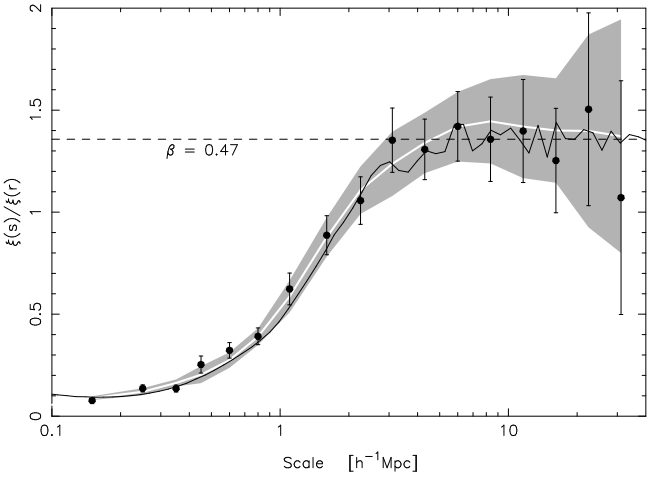

Figure 13. The ratio of $\xi(s)$ to $\xi(r)$ for the 2dF combined data (solid points), and the Hubble Volume simulation (solid line) (Hawkins et al. 2003). The mean of the mock catalog results is also shown (white line), with the rms errors shaded. The error bars on the 2dF data are from the rms spread in mock catalog results.

(Peacock et al. 2001), obtained by Hawkins et al. (2003).

Nonlinear Regime

In the nonlinear regime, the parameter β can be measured by fitting the measured $\xi(r_p, \pi_s)$ (see Sec.4.2) to a phenomenological model (Peebles 1980)

$$\xi(r_p,\pi_s) = \int_{-\infty}^{\infty} \mathrm{d}v\, f(v)\, \tilde{\xi}\left(r_p, \pi_s - \frac{v}{a(z)H(z)}\right), \tag{96}$$

where $\tilde{\xi}(r_p, \pi_s)$ is the *linear* redshift-space correlation function. Hamilton (1992) derived the model for $\tilde{\xi}(r_p, \pi_s)$ by translating Eq.(92) from Fourier space into real space:

$$\tilde{\xi}(r_p,\pi_s) = \xi_0(s)P_0(\mu) + \xi_2(s)P_2(\mu) + \xi_4(s)P_4(\mu), \tag{97}$$

where $P_l(\mu)$ are Legendre polynomials, $\mu = \cos\theta$, with θ denoting the angle between the position vector $\mathbf{r}$ and π_s, and

$$\xi_0(s) = \left(1 + \frac{2\beta}{3} + \frac{\beta^2}{5}\right)\xi(r), \tag{98}$$

$$\xi_2(s) = \left(\frac{4\beta}{3} + \frac{4\beta^2}{7}\right)\left[\xi(r) - \overline{\xi}(r)\right], \tag{99}$$

$$\xi_4(s) = \frac{8\beta^2}{35}\left[\xi(r) + \frac{5}{2}\overline{\xi}(r) - \frac{7}{2}\overline{\overline{\xi}}(r)\right], \tag{100}$$

where

$$\overline{\xi}(r) = \frac{3}{r^3}\int_0^r \mathrm{d}r'\, \xi(r')r'^2, \tag{101}$$

$$\overline{\overline{\xi}}(r) = \frac{5}{r^5}\int_0^r \mathrm{d}r'\, \xi(r')r'^4. \tag{102}$$

The small-scale random motions can be modeled by

$$f(v) = \frac{1}{\sigma_p\sqrt{2}}\,\exp\left(\frac{-\sqrt{2}|v|}{\sigma_p}\right) \tag{103}$$

where σ_p is the pairwise peculiar velocity dispersion. Convolution in real space becomes multiplication in Fourier space, so Eq.(96) becomes

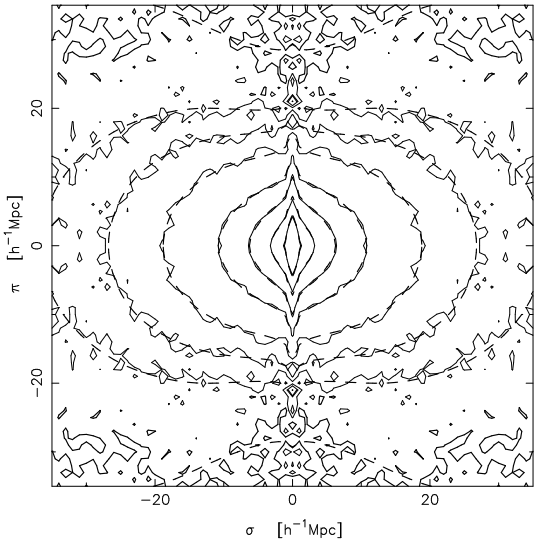

Figure 14. Contours of two-point correlation function $\xi(r_p, \pi_s)$ for the 2dFGRS data (solid lines) and the best-fitting model using the Hubble Volume $\xi(r)$ fitted to scales $8 < s < 30\,h^{-1}$Mpc (dashed lines) (Hawkins et al. 2003). Contours levels are at $\xi = 4.0$, 2.0, 1.0, 0.5, 0.2, 0.1, 0.05, and 0.0 (thick line). Note that the labels $\sigma = r_p$, and $\pi = \pi_s$.

$$P_s(\mathbf{k}) = \hat{f}(k_\parallel) P_s^{lin}(\mathbf{k}) = \hat{f}(k_\parallel) \left(1 + \beta\mu^2\right)^2 P_r(k), \quad (104)$$

where $\hat{f}(k_\parallel)$ is the Fourier transform of $f(v)$ (Hamilton 1998):

$$\hat{f}(k_\parallel) = \int_{-\infty}^{\infty} \mathrm{d}v\, f(v) e^{ik_\parallel v} = \frac{1}{1 + \frac{1}{2}(\sigma_p k_\parallel)^2}, \quad (105)$$

where $k_\parallel = k\mu$.

Fig.14 shows the 2dF two-point galaxy correlation function $\xi(r_p, \pi_s)$, with the redshift-space distortions very clearly indicated. This yielded a measurement of $\beta = 0.49 \pm 0.09$ in a multi-parameter fit to $\xi(r_p, \pi_s)$ (Hawkins et al. 2003). The error bars are determined using the rms spread of results in Mock catalogs. These catalogs are generated from Hubble Volume simulations in the fiducial cosmology.

Guzzo et al. (2007) showed how the estimators of β can be tested for both statistical and systematic errors.

6.2 Measuring the bias factor

In order to measure the growth rate $f_g(z) = b(z)\beta(z)$, we need to measure the bias factor $b(z)$, in addition to the linear redshift-space distortion factor $\beta(z)$. If we know that bias is linear, i.e., $\delta_g(\mathbf{x}) = b\delta_m(\mathbf{x})$, then $b(z) \simeq \sigma_{8,g}/\sigma_{8,m}$ (the ratio of σ_8 for galaxies and matter). Thus $f_g(z)\sigma_{8,m} \simeq \beta(z)\sigma_{8,g}$. The measurement of $\beta(z)$ and $\sigma_{8,g}$ thus provides a measurement of $f_g(z)\sigma_{8,m}$, which can be used directly to test gravity (Percival & White 2009; White, Song, & Percival 2009).

However, it is important to directly measure the bias factor, including its scale-dependence (which is one of the main systematic uncertainties in the BAO scale measurement, see Sec.3.3). This can be done through the comparison of the measured probability distribution function of galaxy fluctuations with theoretical expectations (Sigad, Branchini, & Dekel 2000; Marinoni et al. 2005). Here we focus on another method that utilizes the galaxy bispectrum.

We can assume that the galaxy density perturbation δ_g is related to the matter density perturbation $\delta(\mathbf{x})$ as follows (Fry & Gaztanaga 1993):

$$\begin{aligned}\delta_g &= f[\delta(\mathbf{x})] \simeq b_1\delta(\mathbf{x}) + b_2\delta^2(\mathbf{x})/2 \\ &\simeq b_1\delta^{(1)}(\mathbf{x}) + b_1\delta^{(2)}(\mathbf{x}) + \frac{1}{2}b_2\left[\delta^{(1)}(\mathbf{x})\right]^2. \end{aligned} \quad (106)$$

Thus to second order (Matarrese, Verde, & Heavens 1997)

$$\langle\delta_{g1}\delta_{g2}\delta_{g3}\rangle = b_1^3\left\langle\delta_1^{(1)}\delta_2^{(1)}\delta_3^{(2)}\right\rangle + cyc. + \frac{b_1^2 b_2}{2}\left\langle\delta_1^{(1)}\delta_2^{(1)}\left[\delta_3^{(1)}\right]^2\right\rangle + cyc. \quad (107)$$

where "cyc." refers to the permutations $\{231\}$ and $\{312\}$.

The galaxy bispectrum is defined by

$$\langle\delta_{g\mathbf{k}_1}\delta_{g\mathbf{k}_2}\delta_{g\mathbf{k}_3}\rangle \equiv (2\pi)^3\, B(\mathbf{k}_1, \mathbf{k}_2, \mathbf{k}_3)\, \delta^D(\mathbf{k}_1 + \mathbf{k}_2 + \mathbf{k}_3). \quad (108)$$

Using the expression for $\delta^{(2)}_{\mathbf{k}}$ from Catelan et al. (1995) and Eq.(107), we find

$$\begin{aligned}B(\mathbf{k}_1, \mathbf{k}_2, \mathbf{k}_3) &= \left\{P_g(\mathbf{k}_1)P_g(\mathbf{k}_2)\left[\frac{2J(\mathbf{k}_1, \mathbf{k}_2)}{b_1} + \frac{b_2}{b_1^2}\right] + cyc.\right\}\cdot \\ &\quad \cdot\delta^D(\mathbf{k}_1 + \mathbf{k}_2 + \mathbf{k}_3), \end{aligned} \quad (109)$$

where we have used

$$\langle\delta_{g\mathbf{k}_1}\delta_{g\mathbf{k}_2}\rangle = (2\pi)^3 P_g(\mathbf{k}_1)\delta^D(\mathbf{k}_1 + \mathbf{k}_2), \quad (110)$$

with δ_D denoting the Dirac delta function. Eq.(110) follows from Eqs.(56), (57), (27) and (29). J is a function that depends on the shape of the triangle formed by ($\mathbf{k}_1$, $\mathbf{k}_2$, $\mathbf{k}_3$) in $\mathbf{k}$ space, but only depends very weakly on cosmology (Matarrese, Verde, & Heavens 1997):

$$J(\mathbf{k}_1, \mathbf{k}_2, \Omega_m) = 1 - B(\Omega_m) + \frac{\mathbf{k}_1\cdot\mathbf{k}_2}{2k_1k_2}\left(\frac{k_1}{k_2} + \frac{k_2}{k_1}\right) + B(\Omega_m)\left(\frac{\mathbf{k}_1\cdot\mathbf{k}_2}{k_1k_2}\right)^2, \quad (111)$$

where $B(\Omega_m) \simeq 2/7$ (assuming no coupling of dark enegry to matter), and is insensitive to Ω_m (Bouchet et al. 1992; Catelan et al. 1995).

Verde et al. (2002) applied the galaxy bispectrum method for measuring b_i to the 2dF data. Independent measurements of $\beta(z)$ and $b_i(z)$ have only been published for the 2dF and VVDS data (Hawkins et al. 2003; Verde et al. 2002; Marinoni et al. 2005; Guzzo et al. 2007).

The large-scale infall (parametrized by the redshift-space distortion parameter β, see Eq.[92]) and small-scale smearing (parametrized by the pairwise velocity σ_p) lead to the power spectrum in redshift space (see Eq.[104]):

$$P_s(\mathbf{k}) = P(k)\,\frac{\left(1 + \beta\mu^2\right)^2}{1 + k^2\mu^2\sigma_p^2/2}. \quad (112)$$

Note that σ_p is implicitly divided by H_0. The bispectrum is modified similarly (Verde et al. 2002):

$$\begin{aligned}B_s(\mathbf{k}_1, \mathbf{k}_2, \mathbf{k}_3) &= (B_{12} + B_{23} + B_{31})\left[\left(1 + \frac{\alpha_V^2 k_1^2\mu_1^2\sigma_p^2}{2}\right)\right. \\ &\left.\times\left(1 + \frac{\alpha_V^2 k_2^2\mu_2^2\sigma_p^2}{2}\right)\left(1 + \frac{\alpha_V^2 k_3^2\mu_3^2\sigma_p^2}{2}\right)\right]^{-1/2}, \end{aligned} \quad (113)$$

where $\mathbf{k}_3 = -\mathbf{k}_1 - \mathbf{k}_2$, and $\mu_i = \mathbf{r}\cdot\mathbf{k}_i/(rk_i)$. The adjustable parameter α_V depends on the shape of the triangle, and must be calibrated from simulations (Verde et al. 2002). Also

$$\begin{aligned}B_{12} &= \left(1 + \beta\mu_1^2\right)\left(1 + \beta\mu_2^2\right)\left[\frac{\mathrm{Ker}(\mathbf{k}_1, \mathbf{k}_2)}{b_1} + \frac{b_2}{b_1^2}\right]\cdot \\ &\quad \cdot P_g(\mathbf{k}_1)P_g(\mathbf{k}_2). \end{aligned} \quad (114)$$

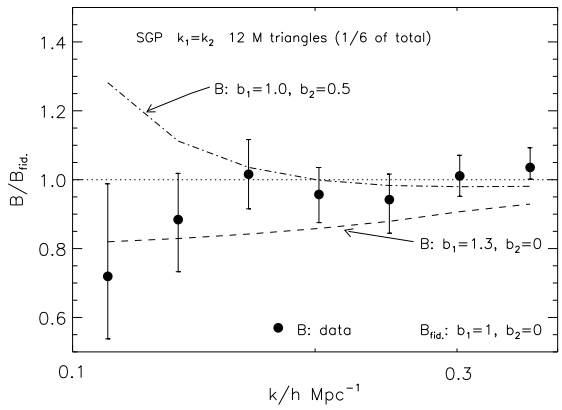

Figure 15. Ratio of the average measured bispectrum from 2dF galaxy redshift survey and the average perturbation theory predictions, relative to the bispectrum for a fiducial unbiased model $B_{\rm fid}$ (Verde et al. 2002). The dashed line corresponds to $b_1 = 1.3, b_2 = 0$, and the dot-dashed line corresponds to $b_1 = 1.0, b_2 = 0.5$. The error bars are obtained via Monte Carlo from 16 mock catalogs, and are placed centrally on the mean of the estimates from the mock catalogs. This illustrates the level of bias in the estimator. The figure shows that there is no evidence of scale dependent bias from the 2dF data.

The kernel function Ker is J modified for redshift space (Verde et al. 1998; Heavens, Matarrese, & Verde 1998):

$$\begin{aligned}{\rm Ker}(\mathbf{k}_1,\mathbf{k}_2) &= J(\mathbf{k}_1,\mathbf{k}_2)b_1 + \mu^2\beta b_1 K^{(2)}(\mathbf{k}_1,\mathbf{k}_2) + \mu_1^2\mu_2^2\beta^2 b_1^2 \\ &+\frac{b_1^2\beta}{2}\left(\mu_1^2+\mu_2^2\right) + \frac{b_1^2\beta}{2}\mu_1\mu_2\left(\frac{k_1}{k_2}+\frac{k_2}{k_1}\right) \\ &+\frac{b_1^2\beta^2}{2}\mu_1\mu_2\left(\mu_2^2\frac{k_2}{k_1}+\mu_1^2\frac{k_1}{k_2}\right), \end{aligned} \quad (115)$$

with $\mu = -\mu_3$, and (Catelan & Moscardini 1994)

$$K^{(2)}(\mathbf{k}_1,\mathbf{k}_2) = \frac{3}{7} + \frac{\mathbf{k}_1\cdot\mathbf{k}_2}{2k_1k_2}\left(\frac{k_1}{k_2}+\frac{k_2}{k_1}\right) + \frac{4}{7}\left(\frac{\mathbf{k}_1\cdot\mathbf{k}_2}{k_1k_2}\right)^2. \quad (116)$$

Eqs.(113)-(115) show how the bispectrum can allow us to measure the bias parameters.

The bispectrum depends on β, $\sigma_{\rm p}$, and $P_{\rm g}$, in addition to the bias parameters b_1 and b_2. The bispectrum and power spectrum data come from Fourier transforming the galaxy number density distribution $n(\mathbf{r})$ through (see the discussion of the FKP method in Sec.4.1)

$$F(\mathbf{r}) \equiv \lambda w(\mathbf{r})\left[n(\mathbf{r}) - \alpha_s n_{\rm s}(\mathbf{r})\right], \quad (117)$$

where λ is a constant to be determined, and $n_{\rm s}(\mathbf{r})$ is the number density of a random catalog with the same selection function as the real catalog, but with $1/\alpha_s$ times ($\alpha_s \leqslant 0.2$) as many particles. The weight $w(\mathbf{r}) = 1/[1 + P_0\bar{n}(\mathbf{r})]$ has been chosen to minimize the variance of higher-order correlation functions (Scoccimarro 2000), where $\bar{n}(\mathbf{r})$ is the average number density of galaxies at position $\mathbf{r}$, and P_0 is the power spectrum to be estimated. Since the results are not sensitive to P_0, it can be chosen to be a constant, for example, $P_0 = 5000\,h^{-3}{\rm Mpc}^3$, to enable the use of a fast Fourier transform. If we set $\lambda = I_{22}^{-1/2}$, where (Matarrese, Verde, & Heavens 1997)

$$I_{ij} \equiv \int {\rm d}^3 w^i(\mathbf{r})\bar{n}^j(\mathbf{r}) \quad (118)$$

then the power spectrum may be estimated from

$$\left\langle |F_k|^2\right\rangle = P_{\rm g}(\mathbf{k}) + \frac{I_{21}}{I_{22}}(1+\alpha), \quad (119)$$

and Eq.(112) can be used to remove the redshift-space distortions. The bispectrum may be estimated from

$$\begin{aligned}\left\langle F_{\mathbf{k}_1}F_{\mathbf{k}_2}F_{\mathbf{k}_3}\right\rangle &= \frac{I_{33}}{I_{22}^{3/2}}\left\{B_{\rm g}(\mathbf{k}_1,\mathbf{k}_2,\mathbf{k}_3) + \frac{I_{32}}{I_{33}}\left[P_{\rm g}(\mathbf{k}_1)+P_{\rm g}(\mathbf{k}_2)+P_{\rm g}(\mathbf{k}_3)\right]\right. \\ &\left. + \left(1-\alpha^2\right)\frac{I_{31}}{I_{33}}\right\}. \end{aligned} \quad (120)$$

It is assumed implicitly that the power spectrum is roughly constant over the width of the survey window function in $\mathbf{k}$-space.

The real parts of $F_{\mathbf{k}_1}F_{\mathbf{k}_2}F_{\mathbf{k}_3}$ are taken as data, for triangles in $\mathbf{k}$ space ($\mathbf{k}_1+\mathbf{k}_2+\mathbf{k}_3=0$). Each triangle yields an estimate of a linear combination of $c_1 \equiv 1/b_1$ and $c_2 \equiv b_2/b_1^2$ (see Eqs.[113] and [115]). Triangles of different shapes (i.e., different ${\rm Ker}[\mathbf{k}_1,\mathbf{k}_2]$) must be used to lift the degeneracy between nonlinear gravity and nonlinear bias (Verde et al. 2002).

Verde et al. (2002) found that $b_1 = 1.04 \pm 0.11$ and $b_2 = -0.054 \pm 0.08$ for the 2dF galaxy redshift survey. Their results were marginalized over β and σ_p. Fig.15 shows their bispectrum measurement from 2dF (Verde et al. 2002).

6.3 Using $f_g(z)$ and $H(z)$ to test gravity

The cause for the observed cosmic acceleration could be an unknown energy component in the universe (i.e., dark energy), or a modification of general relativity (i.e., modified gravity). These two possibilities can be differentiated, since given the *same* cosmic expansion history $H(z)$, the modified gravity model is likely to predict a growth rate of cosmic large scale structure $f_g^{MG}(z)$ that differs from the prediction of general relativity $f_g^H(z)$. The growth rate associated with dark energy, $f_g^H(z)$, depends only on $H(z)$ if dark energy is not coupled to dark matter, and dark energy perturbations are negligible (which is true except on very large scales) (Ma et al. 1999). The growth rate associated with modified gravity, $f_g^{MG}(z)$, depends on the details of how general relativity is modified.

A suitably designed galaxy redshift survey would allow the measurement of the cosmic expansion history $H(z)$ from BAO (see Sec.1), and the growth rate of cosmic large scale structure

$$f_g(z) = \beta(z)b(z) \quad (121)$$

from the independent measurements of the linear redshift-space distortion parameter β (see Sec.6.1), and the bias factor between the galaxy and matter distributions $b(z)$ (see Sec.6.2). The measurement of both $H(z)$ and $f_g(z)$ allows us to differentiate between dark energy and modified gravity.

Fig.16 shows the errors on $H(z)$ and $f_g(z) = \beta(z)b(z)$ for a dark energy model that gives the same $H(z)$ as a DGP gravity model with the same Ω_m^0, for a NIR galaxy redshift survey covering 11,931 (deg)^2, and the redshift range $0.5 < z < 2$ (assuming a conservative nonlinear cut equivalent to $p_{NL} = 0.6$), compared with current data (Wang 2008). We have neglected the very weak dependence of the transfer function on dark energy at very large scales in this model (Ma et al. 1999), and added an uncertainty in $\ln b$ (extrapolated from the 2dF measurement) in quadrature to the estimated error on β.

Fig.16(b) shows the $f_g(z)$ for a modified gravity model (the DGP gravity model) with $\Omega_m^0 = 0.25$ (solid line), as well as a dark energy model that gives the same $H(z)$ for the same Ω_m^0 (dashed line). The cosmological constant model from Fig.16(a) is

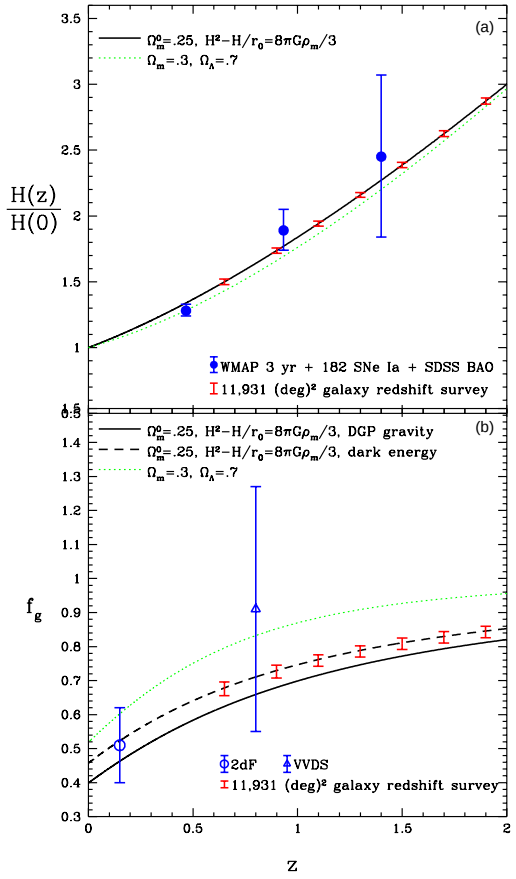

Figure 16. Current and expected future measurements of the cosmic expansion history $H(z)$ and the growth rate of cosmic large scale structure $f_g(z)$ (Wang 2008). The future data correspond to a NIR galaxy redshift survey covering >10,000 square degrees and $0.5 < z < 2$. If the $H(z)$ data are fit by both a DGP gravity model and an equivalent dark energy model that predicts the same expansion history, a survey area of $\sim 14,000\,(\mathrm{deg})^2$ is required to rule out the DGP gravity model at $> 99\%$ confidence level.

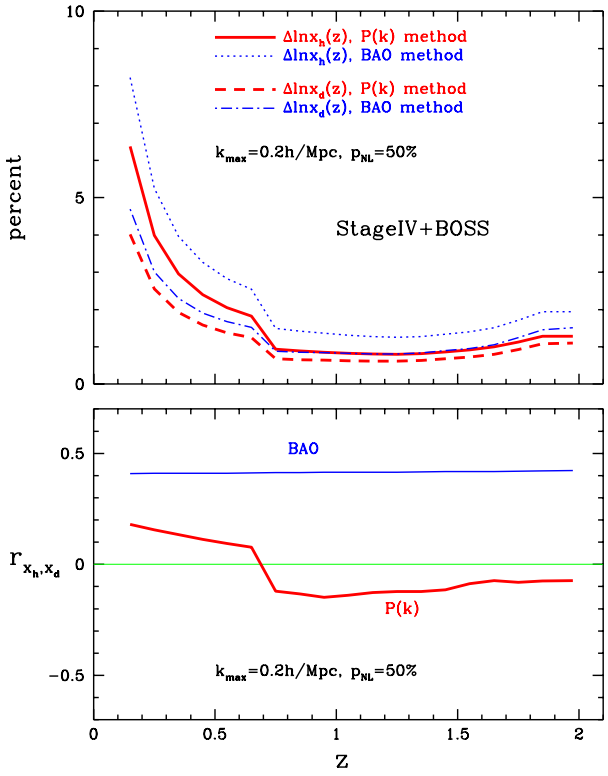

Figure 17. Precision of $x_h(z) \equiv H(z)s$ and $x_d(z) \equiv D_A(z)/s$ expected from StageIV+BOSS. The top panel shows the percentage errors on $x_h(z)$ and $x_d(z)$ per $\Delta z = 0.1$ redshift bin, the bottom panel shows the normalized correlation coefficient between $x_h(z)$ and $x_d(z)$.

also shown (dotted line). Clearly, current data can not differentiate between dark energy and modified gravity. A very wide and deep galaxy redshift survey provides measurement of $f_g(z)$ accurate to a few percent [see Fig.16(b)]; this will allow an unambiguous distinction between dark energy models and modified gravity models that give identical $H(z)$ [see the solid and dashed lines in Fig.16(b)]. A survey covering $\sim 14,000\,(\mathrm{deg})^2$ would rule out the DGP gravity model that gives the same $H(z)$ and Ω_m^0 at $> 99\%$ confidence level (Wang 2008).

Under quite conservative assumptions about systematic uncertainties, a Stage IV galaxy redshift survey, with $0.7 < z < 2$ over 15,000 $(\mathrm{deg})^2$ (e.g., the Euclid galaxy redshift survey), can measure $\{x_h(z), x_d(z), f_g(z)G(z)\tilde{P}_0^{1/2}/s^4\}$ with high precision (where $f_g(z)$ and $G(z)$ are the linear growth rate and factor of large scale structure respectively, and $\tilde{P}_0$ is the dimensionless normalization of $P_g^{obs}(k)$), when redshift-space distortion information is included (Wang 2012). The measurement of $f_g(z)G(z)\tilde{P}_0^{1/2}/s^4$ provides a powerful test of gravity, and significantly boosts the dark energy FoM when general relativity is assumed. Fig.17 shows the measurement precision of $x_h(z)$ and $x_d(z)$ for StageIV+BOSS. The top panel shows the percentage errors on $x_h(z)$ and $x_d(z)$, the bottom panel shows the normalized correlation coefficient between them. The thick solid and dashed lines represent the measurement precision of $x_h(z)$ and $x_d(z)$ from the $P(k)$ method, marginalized over all other parameters. The thin dotted and dot-dashed lines represent the measurement of $x_h(z)$ and $x_d(z)$ from the BAO only method. The top panel of Fig.18 shows the measurement uncertainties on $f_g(z)G(z)\tilde{P}_0^{1/2}/s^4$ and $\beta(z)$ for StageIV+BOSS per $\Delta z = 0.1$ redshift bin. The bottom panel of Fig.18 shows the uncertainties on the growth rate powerlaw index γ for StageIV+BOSS, with and without Planck priors. Note that γ is defined by parametrizing the growth rate as a powerlaw (Wang & Steinhardt 1998; Lue, Scoccimarro, & Starkman 2004),

$$f_g(z) = [\Omega_m(a)]^\gamma\,, \tag{122}$$

where $\Omega_m(a) = 8\pi G\rho_m(a)/(3H^2)$. The solid lines in the bottom panel of Fig.18 show the precision on γ using only the $\{x_h(z), x_d(z), f_g(z)\sigma_m(z)/s^4\}$ measured from $P(k)$ and marginalized over all other parameters. The dashed lines show the precision on γ when the full $P(k)$ is used, including the growth information (i.e., the "$P(k) + f_g$" method).

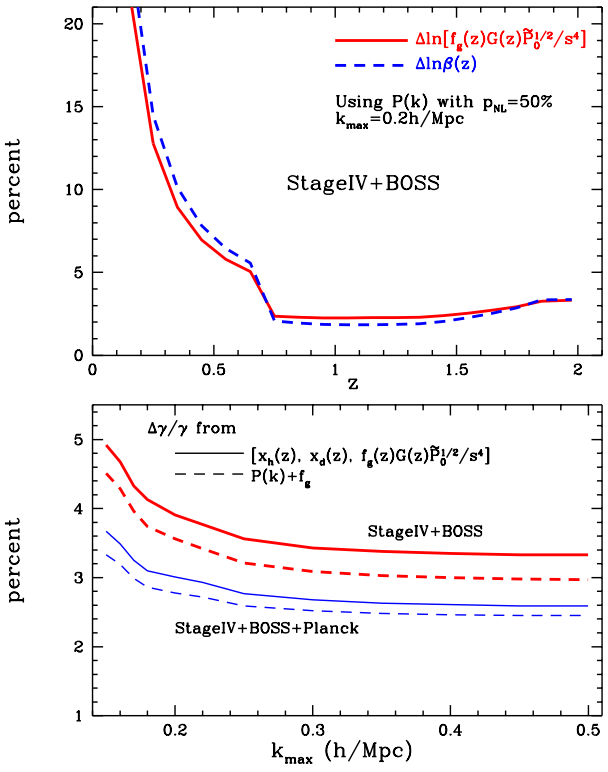

Figure 18. Top: uncertainties on $f_g(z)G(z)\tilde{P}_0^{1/2}/s^4$ and $\beta(z)$ for StageIV+BOSS per $\Delta z = 0.1$ redshift bin. Bottom: uncertainties on the growth rate powerlaw index γ for StageIV+BOSS, with and without Planck priors.

7 THE ALCOCK-PACZYNSKI TEST

Alcock & Paczynski (1979) noted that if an astrophysical structure is spherically symmetric, then its measured radial and transverse dimensions can be used to constrain the cosmological model. A galaxy redshift survey enables the Alcock-Paczynski test to be carried out.

Features in the galaxy power spectrum, such as the BAO, should have the same length scale in the radial and transverse directions. The radial length scale is measured using

$$H(z)\Delta r_\parallel = c\Delta z, \tag{123}$$

where Δz is the redshift interval spanned by $\Delta r_\parallel$. The transverse length scale is measured using

$$\Delta r_\perp = D_A(z)\Delta\theta, \tag{124}$$

where $\Delta\theta$ is the angle subtended by $\Delta r_\perp$.

Thus the Alcock-Paczynski test of requiring that $\Delta r_\perp = \Delta r_\parallel$ leads to

$$\frac{H(z)D_A(z)}{c} = \frac{\Delta z}{\Delta\theta}. \tag{125}$$

This provides a cross check of the measured $H(z)$ and $D_A(z)$ derived from the BAO scale measurements.

Redshift-space distortions (a source of cosmological information themselves) introduce a systematic uncertainty in the Alcock-Paczynski test. Unless properly modeled and removed, redshift-space distortions can alter the measured length scale in the radial direction from galaxy redshift surveys, and bias the Alcock-Paczynski test.

ACKNOWLEDGMENTS

I am grateful to Chia-Hsun Chuang for very useful discussions. This work was supported in part by DOE grant DE-FG02-04ER41305.

REFERENCES

Alcock, C.; Paczynski, B., 1979, Nature, 281, 358
Almeida, C., Baugh, C. M., Lacey, C. G., 2007, MNRAS, 376, 1711
Almeida, C.; Baugh, C. M.; Wake, D. A.; Lacey, C. G.; Benson, A. J.; Bower, R. G.; Pimbblet, K., 2008, MNRAS, 386, 2145
Angulo, R., et al. 2005, Mon.Not.Roy.Astron.Soc.Lett., 362, L25-L29
Angulo, R.E.; Baugh, C.M.; Frenk, C.S.; Lacey, C.G. 2008, MNRAS, 383, 755
Baugh C. M., Lacey C. G., Frenk C. S., Granato G. L., Silva L., Bressan A., Benson A. J., Cole S., 2005, MNRAS, 356, 1191
Baugh, C. M., 2006, Reports of Progress in Physics, 69, 3101
Benson, A. J., Cole, S., Frenk, C. S., Baugh, C. M., Lacey, C. G., 2000, MNRAS, 311, 793
Blake, C., Glazebrook., K, 2003, ApJ, 594, 665
Blake, C., *et al.*, *MNRAS* 365 (**2006**), p. 255
Bouchet, F. R.; Juszkiewicz, R.; Colombi, S.; Pellat, R., 1992, ApJ, 394, L5
Catelan, P.; Moscardini, L., 1994, ApJ, 436, 5
Catelan, P.; Lucchin, F.; Matarrese, S.; Moscardini, L., 1995, MNRAS, 276, 39
Chuang, C.-H.; Wang, Y., MNRAS, in press (2012), arXiv:1102.2251
Cimatti, A., et al. 2009, private communication.
Cohn J.D., 2006, New Astron. Rev., 11, 226
Cole, S., et al., 2005, MNRAS, 362, 505
Crocce M., Scoccimarro R., 2006, PRD, 73, 063520
Crocce M., Scoccimarro R., 2008, PRD, 77, 023533
da Angela, J. *et al.*, astro-ph/0612401.
Davis, M., & Huchra, J., 1982, ApJ, 254, 437
Davis, M.; Peebles, P. J. E. 1983, ApJ, 267, 465
Dick, J.; Knox, L.; Chu, M. 2006, JCAP 0607, 001
Dolney, D., Jain, B., Takada, M.;2006;MNRAS;366;884
Eisenstein, D. J., Hu, W.; 1999;ApJ;511;5
Eisenstein, D., *et al.*, *ApJ* 633 (**2005**), p. 560
Eisenstein D.J., Seo H., Sirko E., Spergel D., 2006b, ApJ, 664, 675
Eisenstein, D.J., et al. 2007, ApJ, 664, 675
Eisenstein D, Hu W;1998;ApJ;496;605
Feldman, H.A., Kaiser, N., Peacock, J.A., 1994, ApJ, 426, 23
Fixsen, D. J., et al., 1996, ApJ, 473, 576
Fry, J. N., Gaztanaga, E. 1993, ApJ, 413, 447
Gaztanaga, E., Cabre, A., & Hui, L. 2008, arXiv:0807.3551
Geach, J.E., et al. 2009, in preparation.
Guzzo L *et al.*, *Nature*, Nature 451, 541 (2008)
Hamilton, A. J. S. 1992, ApJ, 385, L5
Hamilton, A. J. S. 1998, in "The Evolving Universe" ed. D. Hamilton, Kluwer Academic, p. 185-275 (1998), astro-ph/9708102
Hawkins E *et al.*;2003;MNRAS;346;78
Heavens, A. F.; Matarrese, S.; Verde, L., 1998, MNRAS, 301, 797

Hockney, R. W.,& Eastwood, J. W. 1988, *Computer simulation using particles*, Bristol: Hilger, 1988
Hu, W., & Sugiyama, N. 1996, ApJ, 471, 542
Hu, W., Eisenstein, D. J., Tegmark, M.;1998;PRL;80;5255
Hutsi,G. 2006, Astron. & Astrophys., 449, 891
Jeong, D., Komatsu, E,; 2006;ApJ;651;619
Kaiser N;1987;MNRAS;227;1
Kauffmann, G., Nusser, A., Steinmetz, M., 1997, MNRAS, 286, 795
Kendall, M.G. & Stuart, A. 1969, The Advanced Theory of Statistics, Volume II, Griffin, London
Koehler R S, Schuecker P, Gebhardt K;2007;A&A;462;7
Kolb, E.W., Turner, M.S., *The Early Universe*, Addison-Wesley, 1990
Komatsu, E., et al. 2009, ApJS, 180, 330
Landy, S. D., Szalay, A. S., 1993, ApJ, 388, 310
Lewis, A., Challinor, A., and Lasenby, A. 2000, ApJ, 538, 473; http://camb.info/
Lue A, Scoccimarro R, Starkman G D;2004;PRD;69;124015
Ma C P, Caldwell R R, Bode P, Wang L; 1999;ApJ;521;L1
Matarrese, S., Verde, L., Heavens, A. F., 1997, MNRAS, 290, 651
Marinoni, C., et al., 2005, A&A, 442, 801
Matsubara, T. 2004, ApJ, 615, 573
Matsubara T., 2008, PRD, 77, 063530
Mukherjee, P.; Wang, Y., 2003, ApJ, 598, 779; ApJ, 599, 1
Nagashima M., Lacey C. G., Okamoto T., Baugh C. M., Frenk C. S., Cole S., 2005, MNRAS, 363, L31
Nagashima M., Lacey C. G., Baugh C. M., Frenk C. S., Cole S., 2005, MNRAS, 358, 1247
Okumura, T. et al., 2008, ApJ, 676, 889
Orsi, A., et al. 2010, MNRAS, 405, 1006
Padmanabhan, N., White, M., Cohn, J.D., arXiv:0812.2905
Page, L., et al. 2003, ApJS, 148, 233
Peacock, J.A., et al., 2001, Nature, 410, 169
Peebles, P. J. E., 1980, *The Large Scale Structure of the Universe*, Princeton Univ. Press, Princeton, NJ
Percival, W.J., et al. 2007, MNRAS, 381, 1053
Percival, W. J.; White, M., 2009, MNRAS, 393, 297
Reid, B.A., et al., 2012, arXiv:1203.6641
Riess, A. G., et al., ApJ, 659, 98 (2007)
Ross, N. P. *et al.*;2007;MNRAS;381;573
Sanchez, Ariel G.; Baugh, C. M.; Angulo, R. 2008, MNRAS, 390, 1470
Scoccimarro, R., 2000, ApJ, 544, 597
Seljak, U. and Zaldarriaga, M. 1996, ApJ, 469, 437; http://www.cfa.harvard.edu/∼mzaldarr/CMBFAST/cmbfast.html
Seo, H., Eisenstein, D. J., 2003, ApJ, 598, 720
Seo H, Eisenstein D J;2005;ApJ;633;575
Seo, H., & Eisenstein, D. J. 2007, ApJ, 665, 14.
Seo, H., et al. 2008, arXiv:0805.0117
Sigad, Y.; Branchini, E.; Dekel, A., 2000, ApJ, 540, 62S
Smith, R. E., et al. 2003, MNRAS, 341, 1311
Smith, R. E., Scoccimarro, R., Sheth, R. K., astro-ph/0703620
Smith R.E., Scoccimarro R., Sheth R.K., 2008, PRD, 77, 043525
Spergel, D. N., *et al.*, *ApJS*, 170 (**2007**), p. 377
Springel, V., et al., Nature, 435, 629 (2005)
Sumiyoshi, M., et al., arXiv:0902.2064
Tegmark, M.;1997;PRL;79;3806
Tegmark M. et al., 2004, ApJ, 606, 702
Tegmark M. et al., 2006 Phys Rev. D, 74, 123507
Verde, L.; Heavens, A. F.; Matarrese, S.; Moscardini, L., 1998, MNRAS, 300, 747
Verde, L. *et al.*;2002;MNRAS;335;432
Wang, L.; Steinhardt, P.J.;1998;ApJ;508;483
Wang, Y.; Spergel, D.N.; Strauss, M.A., 1999, ApJ, 510, 20
Wang, Y., 2006, ApJ, 647, 1
Wang, Y., 2008b, JCAP0805:021, arXiv:0710.3885 [astro-ph]
Wang, Y., arXiv:0904.2218
Wang, Y., 2012, MNRAS, 423.3631
White, M. 2005, Astropart.Phys. 24, 334
White, M.; Song, Y.-S.; Percival, W.J., 2009, MNRAS, in press; arXiv:0810.1518
Xu, X., et al., 2012, arXiv:1206.6732